

Review

Redox Active Organic-Carbon Composites for Capacitive Electrodes: A Review

Jeanne N'Diaye ^{1,†} , Raunaq Bagchi ^{1,†} , Jane Y. Howe ^{1,2} and Keryn Lian ^{1,*} 

¹ Department of Materials Science and Engineering, University of Toronto, 184 College Street, Toronto, ON M5S 3E4, Canada; jeanne.ndiaye@mail.utoronto.ca (J.N.); r.bagchi@mail.utoronto.ca (R.B.); jane.howe@utoronto.ca (J.Y.H.)

² Department of Chemical Engineering and Applied Chemistry, University of Toronto, 200 College Street, Toronto, ON M5S 3E5, Canada

* Correspondence: keryn.lian@utoronto.ca

† These authors contributed equally to the manuscript.

Abstract: The pressing concerns of environmental sustainability and growing needs of clean energy have raised the demands of carbon and organic based energy storage materials to a higher level. Redox-active organic-carbon composites electrodes are emerging to be enablers for high-performance, high power and long-lasting energy storage solutions, especially for electrochemical capacitors (EC). This review discusses the electrochemical redox active organic compounds and their composites with various carbonaceous materials focusing on capacitive performance. Starting with the most common conducting polymers, we expand the scope to other emerging redox active molecules, compounds and polymers as well as common carbonaceous substrates in composite electrodes, including graphene, carbon nanotube and activated carbon. We then discuss the first-principles computational studies pertaining to the interactions between the components in the composites. The fabrication methodologies for the composites with thin organic coatings are presented with their merits and shortcomings. The capacitive performances and features of the redox active organic-carbon composite electrodes are then summarized. Finally, we offer some perspectives and future directions to achieve a fundamental understanding and to better design organic-carbon composite electrodes for ECs.

Keywords: organic redox active materials; redox active polymers; organic-carbon composite electrodes; capacitive energy storage; electrochemical capacitors; capacitive electrodes



Citation: N'Diaye, J.; Bagchi, R.; Howe, J.Y.; Lian, K. Redox Active Organic-Carbon Composites for Capacitive Electrodes: A Review. *Sustain. Chem.* **2021**, *2*, 407–440. <https://doi.org/10.3390/suschem2030024>

Academic Editor: Matthew Jones

Received: 17 June 2021

Accepted: 23 July 2021

Published: 28 July 2021

Publisher's Note: MDPI stays neutral with regard to jurisdictional claims in published maps and institutional affiliations.



Copyright: © 2021 by the authors. Licensee MDPI, Basel, Switzerland. This article is an open access article distributed under the terms and conditions of the Creative Commons Attribution (CC BY) license (<https://creativecommons.org/licenses/by/4.0/>).

1. Introduction

Electrochemical capacitors (ECs) or supercapacitors, possessing high power densities and excellent cycle life, are one of the key enablers for clean and sustainable energy [1]. From the early conceptual development by Conway [2] in the last century to the latest advancement [3], capacitive materials have been differentiated from battery materials for their fast and reversible charge-discharge kinetics as well as long and stable cycles lives. These properties are originated from two main sources: electrical double-layer capacitance (EDLC) and pseudocapacitance [4,5]. High surface area carbon-based materials are mostly used for EDLC [2,6–10], which store charges through the electrostatic adsorption of ions from the electrolyte on the surface of the electrode. Pseudocapacitance stores and delivers charges through fast and reversible multiple electron transfer oxidation and reduction (redox) reactions [6,11], which can be 10 to 100 times greater than that of EDLC. While pseudocapacitive materials, including metal oxides [12,13], and conducting polymers [14–16], can provide higher specific capacitance and high energy densities, they also add significant cost from materials and processing.

Combining EDLC and pseudocapacitive materials in composite forms is a highly effective, viable and economical approach to leverage the best of both. This has stimulated

significant research and many excellent reviews. Among those reports, the majority are based on carbon modified with metal oxides [1,12,13,17–19] as well as those well-known redox active conducting polymers (CPs) focusing on polyaniline (PANI), polypyrrole (PPy), and poly(3,4-ethylenedioxythiophene) (PEDOT) [20–23]. The inorganic-carbon composites have greatly improved the capacitance and long-term stability of the electrodes, but there are still challenges from environmental and sustainability standpoints, as metal oxides composites still require natural resources and extensive mining and extraction processes.

Although organic materials are abundant and often inexpensive to produce on a large scale, the common electrochemically active (or redox active) materials and composites have been limited to a few conducting polymers. There is a need to explore additional redox active organic compounds to increase the usage of these carbon-based materials and to complement the current capacitive material landscape. Moreover, a strong understanding of the interactions between organic compounds and carbon substrates is important for further development of advanced composites for high performance ECs and other future high power energy storage.

The key for highly capacitive composite electrodes is to leverage and combine the strength of each component to reach the optimal performance or even synergy via rational design and engineering. This review focuses on the electrochemically capacitive composites electrodes based on carbon and promising organic materials. Starting from the well-known conducting polymers, we extend our discussion to other promising redox active molecules and polymers as well as their composites with carbon. Section 2 presents the physicochemical and electrochemical properties of individual key components (i.e., organic layers and carbon substrate) that constitute the composites. Section 3 describes the common approaches to study and develop carbon-organic composites, from computational analyses to fabrication. Section 4 reviews the electrochemical performance of the organic-carbon electrodes, concentrating on thin organic layers on carbon to differentiate from those thick bulk organic composite electrodes. Section 5 summarizes and provides future perspectives.

2. Redox Active Compounds and Carbon Substrates

2.1. Characteristics of Capacitive Materials

The electrochemical performance of capacitive electrode materials is commonly evaluated using cyclic voltammetry (CV), galvanostatic charge-discharge (GCD) and electrochemical impedance spectroscopy (EIS). An ideal capacitive electrode should have a rectangular (for EDLC) or near-rectangular CV profiles with multiple highly reversible faradaic redox peaks overlapped to mimic EDLC (for pseudocapacitance) (Figure 1a). GCD applies a constant current to charge and discharge the electrode and the resulting changes in voltage are linear as shown in Figure 1b [24]. Both capacitive CV and GCD have symmetrical charge/discharge characteristics, which differentiate them from those of battery-like materials [5].

EIS uses a small AC perturbation signal to obtain the impedance as a function of frequency, which can extract the capacitance, equivalent series resistance (ESR), the interfacial, electrolyte, and charge transfer resistance from Nyquist plot (Figure 1c) via equivalent circuit modeling. A Bode plot on phase angle in Figure 1d, gives information on the transition from the resistive to the capacitive dominating frequency region where the phase angle of a capacitive material typically reaches a plateau at around -90° (ideal case). Phase angles lower than -90° can indicate 'leaky capacitor' behavior and possible undesirable side reactions leading to performance decay over time. From EIS measurements, the capacitance of the electrode can be deconvoluted into real (C') and imaginary (C'') portions [25]. The value of C' should be close to the capacitance obtained from DC methods, while C'' is used to identify the transition from resistive to capacitive behavior that occurs at a phase angle of -45° . For capacitive materials, -45° reached at higher frequency is an indication of fast rate [25,26].

Dunn et al. have developed a method to study the kinetics of the dominating charge storage processes by deconvoluting the CV profiles of oxide materials that exhibit inter-

calating capacitance or pseudocapacitance [27,28]. This can be applied to organic-carbon composite electrodes to identify the contributions of different kinetic processes.

One way to do that is to track the peak potential (i) as a function of sweep rate (V) from Equation (1) to obtain the b -value illustrated in Figure 1e. This gives a first qualitative estimation of the dominating charge storage processes as surface-controlled (capacitive) or diffusion-controlled within the composite. As an indication, b -values between 0.8–1 represent highly capacitive materials, while b -values approaching 0.5 imply semi-infinite diffusion control.

$$i = aV^b \quad (1)$$

The surface capacitive and diffusion-controlled processes can be further quantified (Figure 1f) and differentiated using Equation (2) [29], where k_1V represents the capacitive current and $k_2V^{1/2}$ is the contribution from the diffusion current.

$$i(V) = k_1V + k_2V^{1/2} \quad (2)$$

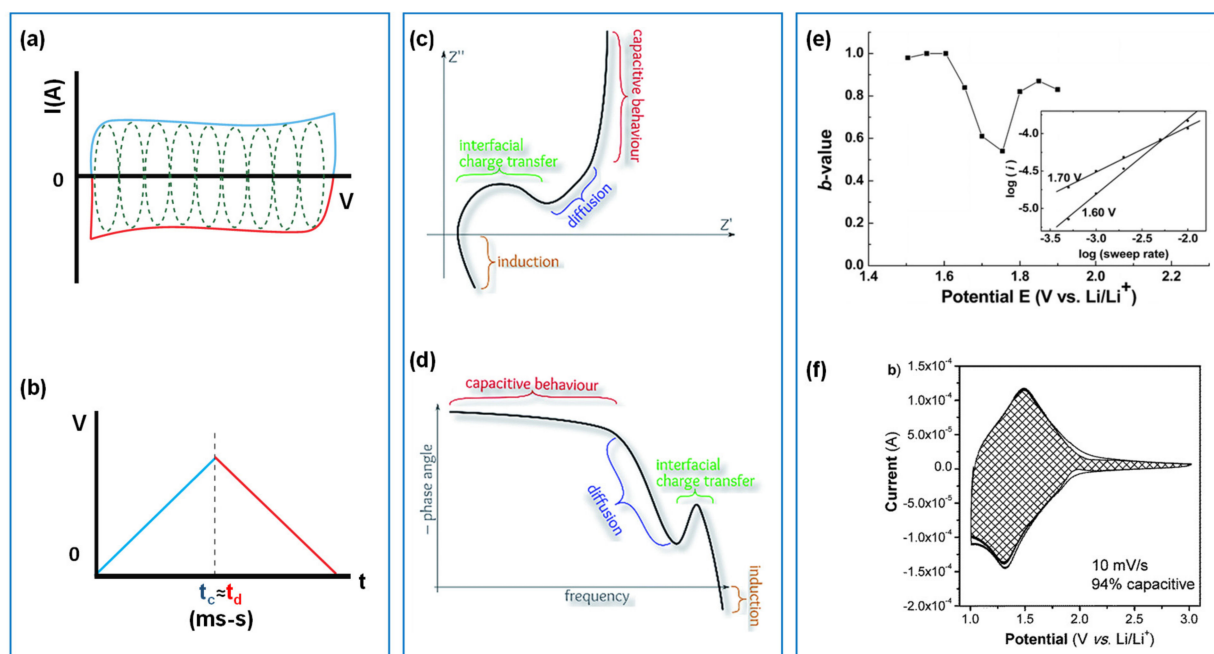


Figure 1. (a,b) CV and GCD profiles, (c,d) Nyquist and Bode plots of capacitive materials, and (e,f) Kinetics analysis of the electrochemical response: b -values and deconvoluted CV profile for intercalating pseudocapacitive materials, reproduced with permission from Refs. [24,26,27,29].

2.2. Electrochemically Active Organic Materials

2.2.1. Redox Active Polymers

The current landscape covering organic energy storage materials are mostly redox conducting polymers (CPs) including, polyaniline (PANI), poly(pyrrole) (PPy), Poly(3,4-ethylenedioxythiophene) (PEDOT), and their derivatives. Redox active CPs contain π -conjugated backbones with alternating single (C-C) and double (C=C) bond carbon [30]. Their chemical versatility, tunable conductivity, reversible electrochemical processes, controllable nanostructure, and low-cost synthesis make them very promising for energy storage [21,30]. The conductivity of the polymer can be tuned via various positive (p) or negative (n) dopants. The p-type dopants include electron-accepting species such as Br_2 , I_2 , H_2SO_4 , HClO_4 , NO_2 , NO^+ , SbCl_6^- , SO_3 , and FeCl_3 [31–33], while n-dopants are sodium naphthylidene, Na/K alloy, molten potassium, etc. The positive-doping (p-doping) in CPs removes electrons from the highest occupied molecular orbital (HOMO) of the conjugated polymers by an electron acceptor, resulting in the polymer at a different oxidized state with orders of magnitudes

increase in conductivity [34]. Using PPy as an example, Figure 2a,b illustrate this process, where the energy gap between HOMO and the lowest unoccupied molecular orbital (LUMO) can vary by the concentration of the dopant. Thus, counter ions or dopants have a significant effect on the electrochemical behavior of CPs, which are mostly in the p-doped state. These oxidized polycations in CPs attract the anions from the electrolyte to intercalate into the polymer backbone for electro-neutrality (Figure 3) [35]. Such highly reversible electrochemical processes enable CPs to be stand-alone pseudocapacitive electrode materials with high specific capacitance.

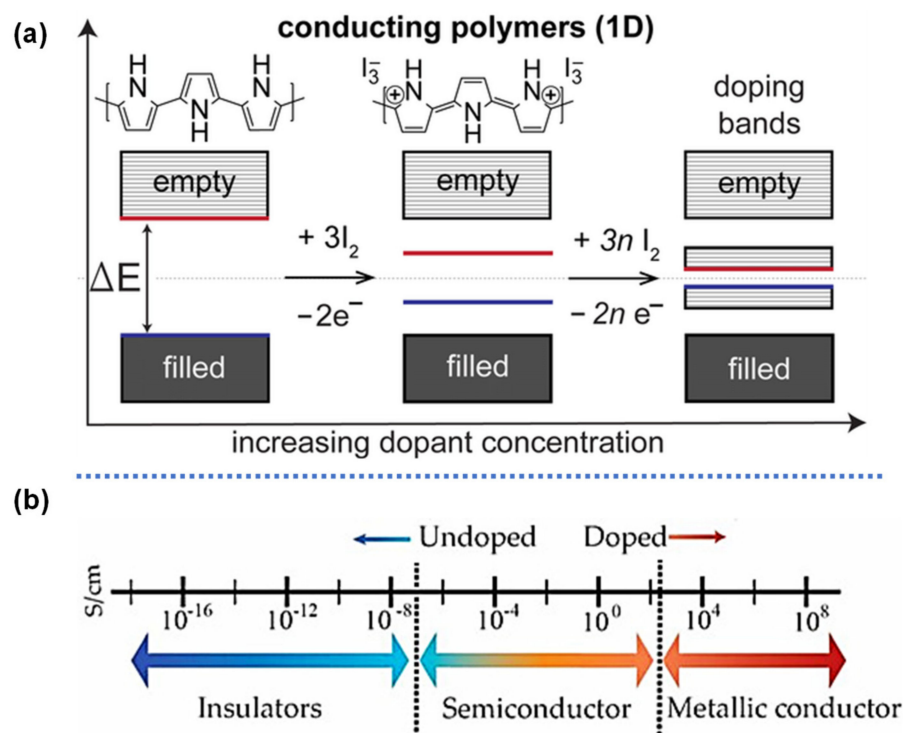


Figure 2. Schematic of (a) molecular orbital of conducting polymers during p-doping and n-doping (example of PPy), and (b) range of conductivities for CPs in their doped and undoped forms, reproduced with permission from Refs. [30,35].

Numerous studies from the literature reviewed and reported the electrochemical redox behaviour and high capacitances of CPs [35–39], e.g., 964–2000 F/g for PANI [40,41], 620 F/g for PPy, and 210 F/g for PEDOT-PSS [42]. In spite of these high values, CPs suffer from stability issues over long-term cycling. The mechanical stress due to the volumetric change of the CPs during the electrochemical cycling leads to cracks, material loss, and degradation [43]. Therefore, composites with carbon nanomaterials have been the main approach to mitigate these shortcomings [16].

2.2.2. Redox Active Organic Compounds

Many other electrochemically active polymers, COFs [44] as well as organic compounds have also demonstrated pseudocapacitive properties. Some promising examples include pyrenes derivatives [45,46], meta, para and ortho (m, p, o)-phenylenediamines [47–49], quinones [50–52], as well as porphyrin and phthalocyanine macrocycles [53–56]. The advantages of these molecules are their chemical tunability and their nitrogen and oxygen redox functional groups that can undergo reversible charge transfer processes (Table 1). For instance, quinone based molecules have a high theoretical capacity, fast electron transfer kinetics, and low-cost synthesis [57]. Their redox activities stem from the reversible conversion of the quinone groups to hydroxyl groups (Figure 4a). However, the quinone groups become unstable in electrolytes with pH greater than 7 [52], indicating that the

redox activities of organic compounds also are electrolyte dependent. This is a critical point since the electrolyte system plays an importance role in the performance of the final composite electrode.

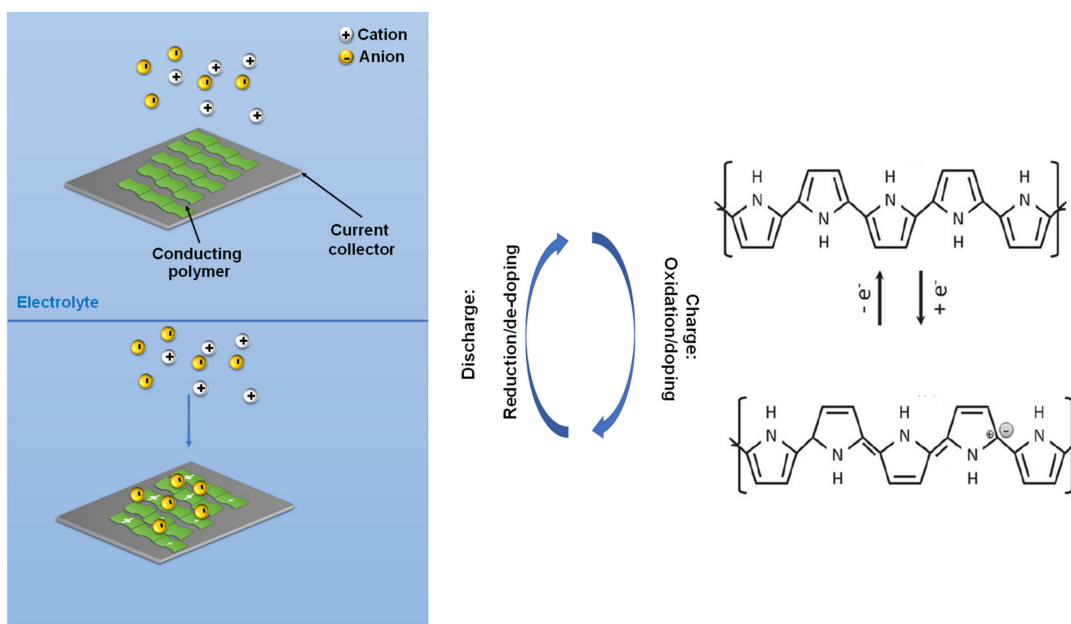


Figure 3. General oxidation and reduction mechanisms for conducting polymers, using PPy as example [30].

Table 1. The redox center of in common electrochemically active organic materials.

Structures	Redox Mechanism	Examples	References
Amine	$\text{R}-\overset{\text{H}}{\underset{\cdot}{\text{N}}}-\text{R} \xrightleftharpoons[+e^-]{-e^-} \text{R}-\overset{\text{H}}{\text{N}}-\text{R}$	PANI, PPy	[39,58]
Carbonyl	$\text{R}-\overset{\text{O}}{\parallel}{\text{C}}-\text{R} \xrightleftharpoons[+e^-]{-e^-} \text{R}-\overset{\ominus}{\text{O}}-\text{C}-\text{R}$	Quinone	[59]
Thioether	$\text{R}-\text{S}-\text{R} \xrightleftharpoons[+e^-]{-e^-} \text{R}-\overset{\oplus}{\text{S}}-\text{R}$	PEDOT	[60,61]
Nitroxyl radical	$\text{R}-\overset{\cdot}{\text{O}}-\text{N}-\text{R} \xrightleftharpoons[+e^-]{-e^-} \text{R}-\overset{\ominus}{\text{O}}-\text{N}-\text{R}$		[62]

The electrochemistry of phenylenediamine (PD), a small molecule with two primary amines attached to the benzene ring is greatly influenced by their different positions. When a second amine group is in the para- or ortho- position, a greater redox current has been observed, attributed to the different hybridization state of the molecules. When para-phenylenediamine (p-PD) and ortho-phenylenediamine (o-PD) are in acidic environment, both can undergo reversible redox processes between the benzoid diamine and quinoid diimine with four resonance structures. Meanwhile, meta-phenylenediamine (m-PD) does not form the quinoid diimine, resulting to a lesser faradaic contribution to the charge storage process (Figure 4b) [48].

Another class of redox organic compounds are polycyclic aromatic hydrocarbon (PAH) such as pyrene, bi-products from fractional distillation process of crude oil and coal tar (Figure 4c) [45]. Due to their π -conjugated structure, the HOMO and LUMO levels of pyrenes and derivatives can be adjusted by electron donors or acceptors of different

strengths, resulting in a range of photophysical and electrochemical properties [63]. Their redox behavior depends on both the electrolyte environment and the redox active moieties attached to their core [64,65].

Recently, Russell et.al. reported a highly pseudocapacitive organic network perylene diimide–hexaazatrinitraphthylene (PHATN) system that possess high capacitance of 689 F/g, excellent stability over 50,000 cycles, and the highest rate capability of 75 A/g [66]. The keys for these successful performances are: (1) the selection of complementary electroactive components that expands the voltage range and thus the charge-storage capacity of the system; and (2) the contortion of the aromatic surface contributing to the pseudocapacitive behaviour, which opens space for electrolyte and ions movement for high rate.

Macrocyclic compounds such as porphyrin and phthalocyanines that have a large π -conjugated system containing up to 22 electrons are redox active (Figure 4d), and commonly used in the field of sensors and thin film transistors [67–74]. The electrochemical behavior of these macrocycles is affected by the position, the number or the type of substituents on the ring, and the coordinated central metal ions [70,75]. With their small HOMO and LUMO gaps, porphyrin and phthalocyanines can act as bipolar organic electrodes by donating or accepting electrons at its mesomeric core with fast redox kinetics [53,76]. The electrochemical redox activities of porphyrin and phthalocyanine are attributed to multiple factors, including the pyrrole-like ring structure, the various substituents, and the coordinated central metal ions in the case of metalloporphyrin. The nitrogen groups of the pyrrole-like structures can have multiple oxidized and reduced states during electrochemical processes [77]. Metal-free porphyrin macrocycles can be reversibly protonated at the pyrrole-like groups to form mono- (H_3TPP^+) and di- (H_4TPP^{2+}) cations leading to the delocalization of one or two electrons in the porphyrin ring [78–80]. However, the underlying mechanism in capacitive charge storage still needs further investigation.

Covalent organic frameworks (COFs) are an emerging class of large porous, crystalline, organic frameworks composed of covalently bonded repeating organic units with wide varieties of functional groups and structures (Figure 4e) [81]. COFs possess 2D conjugated layers arranged in perpendicular nanosheets with 1D pore channels [82]. The development of COFs for composite electrodes in supercapacitors arise from their highly ordered porosity, significant chemical stability, large surface areas, and extensive backbone customizability to incorporate various redox active centers for pseudocapacitive contributions.

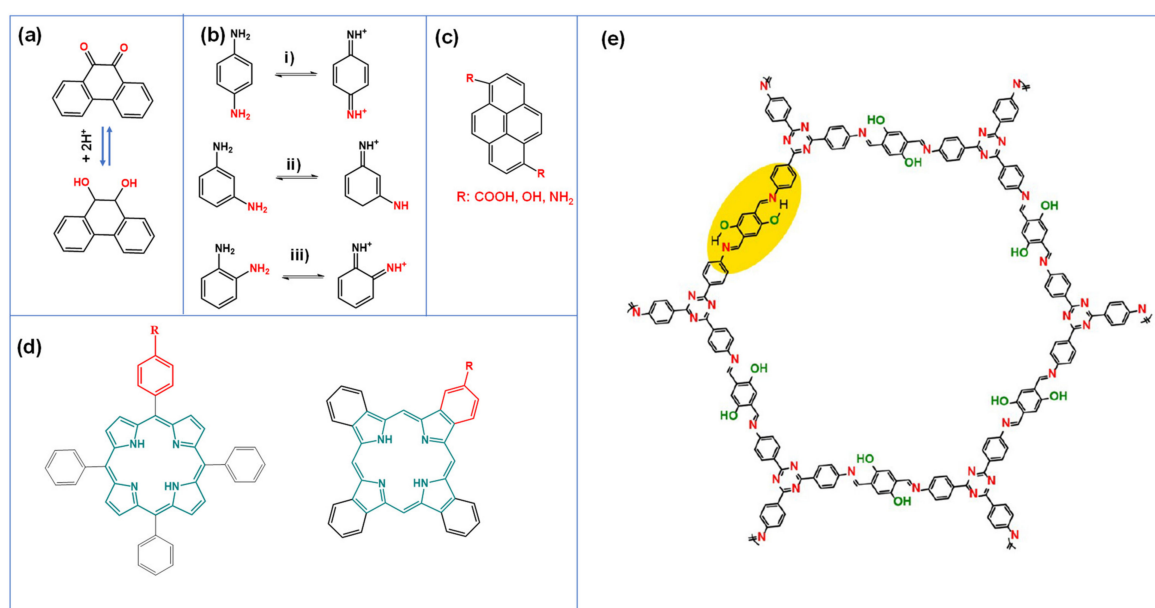


Figure 4. Chemical structure and some redox processes for (a) quinone type molecule, (b) p (i), m (ii), and oPD (iii), (c) pyrene molecules with different redox groups, (d) porphyrin and phthalocyanine macrocycles, and (e) N and O-containing COF. Reproduced with permission from Refs. [45,48,83,84].

2.3. Carbon Substrates for Composite Electrodes

Carbonaceous materials have been the choice of electrode materials for ECs due to their own double-layer properties, in particular carbon allotropes that include biomass activated carbon (AC), carbon nanotubes (CNTs), graphene and carbon nano-onions (Figure 5) [85–90]. Their intrinsic high surface area, adjustable pore structure and size distribution, good electrical conductivity, and chemical stability make them excellent substrates to anchor various type of redox active compounds for high performance electrodes. Furthermore, functional groups on the carbon substrate can contribute towards surface wettability, better electronic activity, pseudocapacitance and enlarged operating potential window [91]. Among surface functional groups, oxygen and nitrogen functionalities are often involved and can be introduced through oxidation, doping or using heteroatom-containing precursors. Other functionalities including sulphur [92], phosphorus and boron, alter the electronic properties of the surface according to their sizes and electronegativities [92–94].

Graphene (Figure 5a), a single-atom-thick layer of sp^2 carbon atoms densely packed into a two-dimensional (2D) hexagonal lattice [95], can be produced via mechanical, chemical vapor deposition, epitaxial growth and electrochemical synthesis [96]. Graphene has a theoretical surface area of $2675 \text{ m}^2/\text{g}$. However, this value decreases to $400\text{--}900 \text{ m}^2/\text{g}$ once the graphene layers are stacked to form an electrode with a uniform mesopore distribution [96–98]. The large-scale production of clean graphene monolayers is still a challenge. The chemical exfoliation of graphite can produce large amounts of graphene oxide (GO), which is a layer of graphene containing various oxygen functionalities. GO is then reduced to rGO to approach the properties of pristine graphene. The use of rGO is advantageous as it can be readily dispersed in aqueous or organic solvents [99].

CNTs (Figure 5b) have a cylindrical shape with sp^2 hybridized carbon atoms. Their good electrical and thermal conductivities, together with reasonable surface area of about $400 \text{ m}^2/\text{g}$ make CNTs excellent substrates to study the electrochemical properties of novel redox active materials [100]. Although their conductivities and surface area are lower than graphene, CNTs, especially multiwalled CNTs, are a lower cost alternative to graphene as substrates for pseudocapacitive molecules and compounds. Nevertheless, the cost of CNT and graphene are still too high which limits their commercial usages.

A wide variety of AC (Figure 5c) have been used for commercial EDLC devices, partially due to their abundance and low-cost. ACs can be produced from different sources including coconut shell, wood, and other biomass waste through a 2-step process: thermal pyrolysis, and activation. This leads to a wide pore size distribution of micropores ($<2 \text{ nm}$), mesopores ($2\text{--}50 \text{ nm}$), and macropores ($>50 \text{ nm}$) in AC structure. In addition to the low-cost, AC possess high chemical stability and high specific surface area up to $3000 \text{ m}^2/\text{g}$ resulting in specific capacitance ranging from $70\text{--}200 \text{ F/g}$ [101–104]. Developing sustainable approaches to produce high performance AC materials is critically important to today's carbon neutrality and is still an ongoing challenge being researched extensively.

The main issue pertaining to carbon substrates is controlling surface features, such as the pore size, shape, and surface functionalities to enable bonding redox active species and promote a high utilization of their redox centre. For instance, leveraging the inherent porosity of waste biomass and improving the interlayer spacing of graphene sheets could be strategies to facilitate molecules and polymers onto the substrate surface [85,105]. Incorporating surface functionalities to the carbon substrate could aid in anchoring organic redox materials and further improve the charge storage properties.

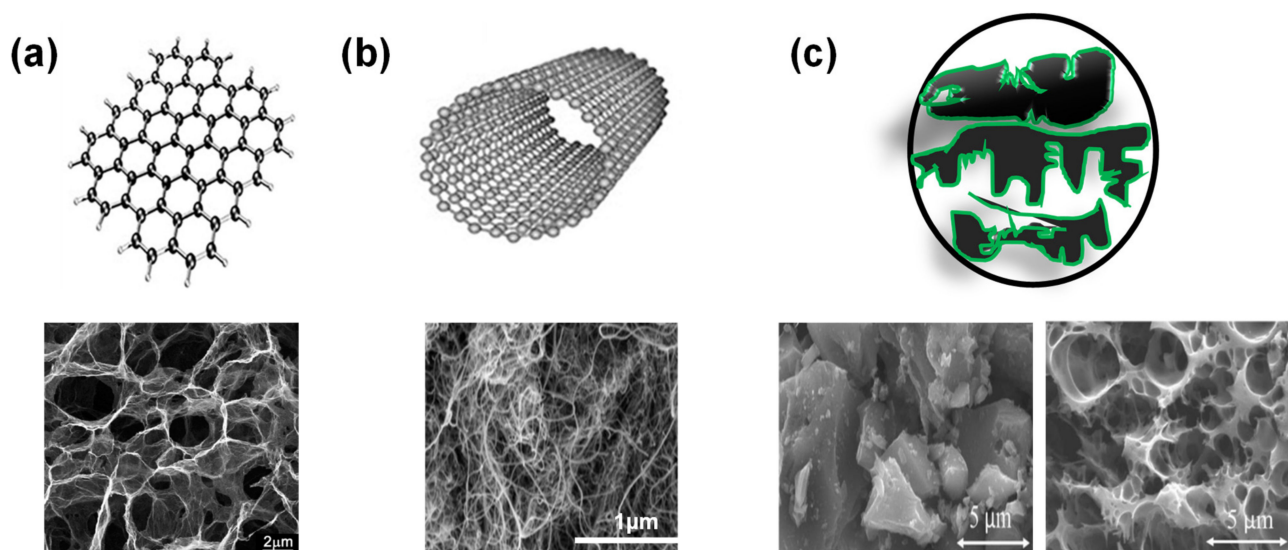


Figure 5. Structures and SEM micrographs of (a) graphene, (b) CNT, and (c) activated carbon: obtained from coconut shell and chitosan biomasses, reproduced with permission from Refs. [88,102,106–108].

3. State-of-the-Art of Redox Active Organic-Carbon Composites

Applying organic redox active material onto carbonaceous materials is commonly practiced in energy storage. What is important in capacitive energy storage is to maintain the pseudocapacitive properties, i.e., fast and reversible charge transfer kinetics and long-term stability for high power and cycle life while enhancing the capacitance and reducing the cost. This needs properly matched and rationally designed composites to leverage the strengths of each component to achieve ideal combination or even synergy. In this section, we start with a review of the fundamental interactions within the composites through first principles studies in Section 3.1, followed by a survey on the prominent fabrications of composite electrodes in Section 3.2.

3.1. Computational Studies of the Interfacial Interactions between Components

Redox active species such as small molecules, macrocyclic compounds, and polymers can be coated or functionalized on a carbon substrate to form composites via different means. The physical and chemical stability of these composites would determine their viability for supercapacitor applications. Computational first-principles studies have been used to predict and model the interactions between the components with these composites [109] and possible interaction mechanisms to support the experimental results. The tools include quantum mechanical approximations such as density functional theory (DFT) or classical approaches such as molecular dynamics (MD) [109].

3.1.1. Noncovalent Interactions

Most of the capacitive organic-carbon composites rely on noncovalent interactions between the electroactive layers and carbon substrate such as van der Waals (vdW) forces, polymer wrapping, hydrogen bonding, and electrostatic interactions [110,111]. The adsorption energies for noncovalent interaction have been quantified through DFT and can vary widely but is generally between ~ 10 – 251 kJ/mol (0.10–2.59 eV) (Figure 6a) [112,113].

- Quantum chemical simulations

DFT studies provide adsorption energies, molecular conformation as well as molecular orbital energy levels. Such parameters are important to understand how the molecules deposit and how they interact with the substrate in terms of overall geometry and electronic configurations of the composite electrodes. However, DFT is limited to systems of approximately 500 atoms [114], so that most studies focused on small molecules, monomeric units (aniline), and pyridine on graphene, rGO or coronene are preferred [115,116]. Meanwhile,

Ab initio molecular dynamics (AIMD) has been used to study the mechanistic pathways of adsorbed molecules, such as aniline and acetonitrile on graphene [117]. From the AIMD results, aniline adsorbed onto graphene had a strong adsorbate binding energy of 69.4 kJ/mol. In addition, the space between the aniline molecule and the graphene layer quickly reached equilibrium at an estimated 3.4 Å in 30 ps, after initially being 6.4 Å apart, consistent with noncovalent interactions (Figure 6b).

Significantly larger redox active molecules such as porphyrin macrocycles and COFs are becoming more prevalent in composites. Tetraphenyl porphyrin sulfonate (TPPS) on CNT was modeled in a DFT study demonstrating Van der Waals-dominated physisorption. Furthermore, the decreased HOMO-LUMO energy gap predicted for TPPS on CNT was related to the improved charge storage and kinetics [118]. A DFT-based study on COFs by Mohammed et al., had shown an improved conductivity for a 2,6-Diaminoanthraquinone and p-toluene sulfonic acid (DqTp)-based COF by forming a π - π interaction with carbon nanofibers (CNFs) (Figure 6c,d) [81]. The per layer stabilization energy is shown to increase significantly from 349 kJ/mol for pristine COF to 1414 kJ/mol for the parallel planar arranged COF-CNF.

On carbon nanotubes or substrates consisting of curved graphene surfaces, diphenylamine exhibited a higher adsorption energy of 116.5 kJ/mol with higher aromatic ring count relative to the 68.8 kJ/mol of single ring aniline [119]. Moreover, the energetic stability, when aniline was positioned on the inside rather than the outside surface of single walled CNT, led to greater binding energies of 68.8 kJ/mol compared to 44.5 kJ/mol. This is rationalized by the larger overlap of HOMO and LUMO regions of aniline on the concave graphene relative to a flat graphene surface as shown in Figure 6e,f [119]. For irregular, porous substrates like ACs, the surface can be approximated to be curved, defective graphene sheets. DFT modeling of defective graphene has been correlated to the adsorption of hydroquinone on AC [120]. The study showed that among varying defects, single-vacancies with dangling bonds have shown better adsorption of hydroquinone and was consistent with the strong adsorption observed within the internal pore walls of the AC.

DFT studies concerning polymers such as polyaniline [121] and polypyrrole [122] have predicted π - π intermolecular interactions and London dispersion forces with physisorption on carbon substrates, but these approaches are limited for larger systems (>1000 atoms) because of the computational cost per atom [114]. In addition, considerations for thermodynamic quantities such as entropy and enthalpy with the motion of species need to be taken into account for a better mechanistic understanding of adsorption and composite interface stability [123]. These challenges make classical methods useful alternatives for studying noncovalent interactions in composites.

- Classical methods

For larger scale simulations of composites such as polymers or large biomolecules, classical simulation methodologies including atomistic molecular dynamics (MD) and classical Monte Carlo (MC) methods which require considerations of nuclear motion [109]. These approaches can accommodate electrolyte interactions for the electric double layer effect but still need further development for pseudocapacitive effects [109,124]

For polymers adsorbed on graphene sheets [125], CNT [126] MD has been used for modeling composites at a good accuracy-computational cost ratio. For example, Yang et al. used MD to simulate the wrapping effect of polymers with different monomeric units on SWCNT, depicting that polymers with aromatic rings in the backbone rather than the side chains have stronger interactions with SWCNTs [126].

The reactive force field interatomic potentials (ReaxFF) approach within MD has enabled the classical treatment of reactive chemistries with considerations for bond orders [127,128]. Using MD with ReaxFF, Benda et al. demonstrated the distribution in adsorption energies for polyfluorene and fluorene/carbazole copolymers with various functional groups noncovalently binding to CNT [129]. The study showed the effects of π - π stacking, and steric repulsion effects between different polymer chains on the stability

of the composite, as shown in Figure 6g Adsorption energies per monomer in the range of 115.9 to 190.8 kJ/mol were calculated for a range of CNT diameters and polymer lengths. This approach can provide insights into the stability of promising redox active polymers on a carbon substrate prior to experimental investigations.

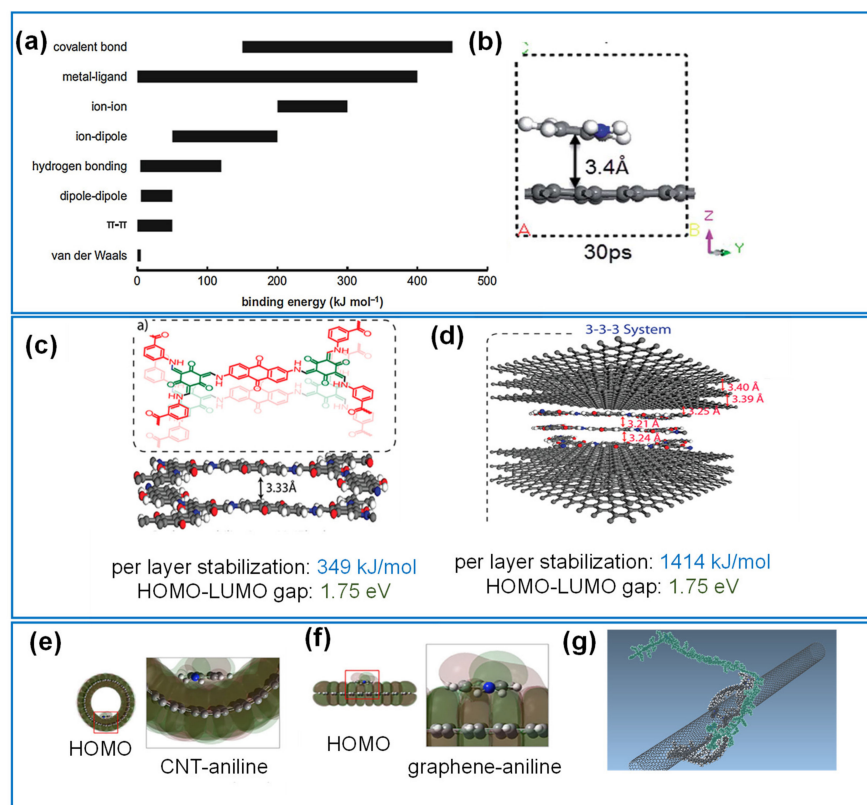


Figure 6. Simulation of the interactions between redox active molecules with carbons. **(a)** Binding energies of different types of interactions. Noncovalent interactions include vdW, π - π , H-bonding, ion-dipole and ion-ion types. **(b)** Interaction configurations of graphene-PANI system via AIMD from 5 ps to 30 ps time frames. **(c)** DFTB model structures of DqTp COF, and **(d)** graphene and 3-3-3 COF-planar. HOMO and LUMO structures of aniline bound to the **(e)** inner surface of the CNT, and **(f)** to flat graphene. **(g)** Two fluorene/carbazole copolymers demonstrating inter-chain steric hindrance. Reproduced with permission from Refs. [81,117,119,129,130].

3.1.2. Covalent Interactions

Covalent bonding of species onto the carbon substrate or chemisorption often leads to more chemically and thermally stable composites. The interaction energies vary between 100–400 kJ/mol, which is usually an order more than that for non-covalent interactions [113]. Covalent bonds, unlike weaker interactions, often form sp^3 structures from the pristine sp^2 configuration of the carbon substrate such as graphene [110], resulting in a less reversible structural change compared to noncovalent interactions. DFT-based quantum mechanical approaches commonly serve as adequate tools for approximating the formation and stability of covalent bonds in the composites, including bond dissociation energies, transition states during the grafting reactions on the surface of the carbon HOMO-LUMO gaps, electronic behavior and surface conformations for these adsorption scenarios.

Atomistic computational investigations of polymerization or chemical grafting on carbon substrates have been performed with small molecules such as pyrenes [131], diazonium cations [132], triazine [133] and biopolymers such as chitosan [134]. This form of bonding between components of a composite commonly requires a more involved fabrication process relative to non-covalently attached composites.

3.2. Fabrication Methods

Among numerous polymerization and deposition methods developed for capacitive composite electrodes, this review will focus on the most common and scalable ones as well as their advantage, and issues. The conditions that affect the successful deposition/polymerization, the nano and microstructures and some inherent properties will also be discussed.

3.2.1. Electropolymerization

The electropolymerization of redox active organic compounds has been the most widely used method. It applies an electrical energy to the electrode immersed in a monomer solution, which is simple, fast, versatile, environmentally benign, and applicable to most redox active polymeric materials. Changes in the polymerization conditions, e.g., monomer concentration, electrode potential, current density, and electrolyte pH will impact the morphology and properties of the polymer [135]. Each type of monomer has an optimal oxidation potential and current for homogeneous polymerization on the substrates. The techniques frequently used in polymerization include potential cycling, potentiostatic steps, and galvanostatic constant current [135].

The electropolymerization of redox active species starts with the oxidation of monomers at a specific potential, followed by the formation of cation radicals of monomers that react with adjacent monomers to form oligomeric products. The process continues during the elongation phase to finally form the polymer chain. The synthesis and doping in polymers are believed to take place simultaneously. The use of electric power supply and the small-scale production of material are the main limitations of electropolymerization.

The charge storage of the electrodes is sensitive to the applied potential during the electrochemical deposition. Zhu et al., showed that increasing the polymerization potential of poly(thieno [3,2-b] thiophene) (PTT) to 1.3 V 1.5 V and 1.7 V led to rougher surface with the formation of nanoparticles. At the polymerization potential of 1.7 V, the capacitance was the highest (627.5 F/g, 15 A g⁻¹) compared to those for the lower polymerization potential [136]. In another example, the chronoamperometric deposition of PEDOT-PSS on graphene produced wrinkled paper-like sheets at a moderate potential of 1.2 V yielded a higher specific capacitance than at 2 V [137,138].

The structure, porosity and chemical composition of the substrate can also affect the microstructure and the electrical conductivity of the polymers [135]. On activated carbon, the organic layer tends to deposit inside the pores which could lead to a decrease in pore size and less available space for ion adsorption. In addition, surface functionalities of the carbon substrate can also play an important role as demonstrated by Branzoi et.al, that the presence of negatively charged oxygen functional groups on the carbon served as anionic dopant during the electropolymerization leading to a better conductivity of the overall composite [139].

3.2.2. In-Situ Chemical Polymerization

In-situ chemical polymerization is also widely used to deposit functional redox active polymers on carbons. The polymerization occurs in solution containing monomers and an oxidizing agent. During the reaction, the monomers diffuse and adsorb on the substrate, and the polymerization is driven by the oxidizing agents [140]. Relatively strong chemical oxidants (initiator) are utilized, including ammonium peroxydisulfate (APS), permanganate or bichromate anions, ferric ions, Mg-H⁺, and hydrogen peroxide [141]. The reactions can occur in aqueous acidic and non-aqueous environments, depending on the solubility of the monomer. Different from electropolymerization, only chemical energy is consumed to produce the final products. However, safety issues can arise from the use of strong oxidizing agents in acid environment. The reaction conditions, e.g., the concentration ratio of monomer/oxidant and reaction environment such as the temperature and pH, etc., also need to be optimized to obtain a consistent and reproducible deposition [142].

In chemically polymerized composite electrodes, the polymer and substrate are mostly connected via non-covalent bonding through π - π , hydrogen bond or sometimes electrostatic bonding [110,143]. Redox active compounds have different orientations and morphologies from the carbon nanostructures. When polymerized on CNT in a controlled environment, PANI and derivatives can wrap around the individual nanotube in thin layers and form a stable composite with long cycling stability [107]. In the case of graphene, the monomeric units tend to intercalate between the graphene nanosheet increasing the interlayer spacing [144].

In-situ polymerization can also involve covalent bonding between the redox active organic compounds and the substrates. Diazonium salt on carbon is one of the good examples [145]. The diazonium grafting has been employed to covalently modify the surface of carbon with conducting polymers, quinones, porphyrin, small organic molecules [59]. This method relies on aryl diazonium salt attached to the organic moieties and bond to carbon. A spontaneous reduction of the diazonium cations occurs on the carbon surface, leading to covalent bonds [146]. Pognon et al., investigated the effects of the covalent grafting of catechol on the surface area and pore distribution of AC, where a difference in deposition mechanisms was found for chemically grafted and physically adsorbed catechol. The former caused a decrease in the accessible pores for ions in the electrolyte, while the latter affected mostly the micropores [59]. With diazonium chemistry acting as covalent linkers, Liu et al., developed a 3D hybrid electrode by grafting PANI nanorods on reduced graphene oxide nanosheets, without the need for binders [147].

3.2.3. Hydro/Solvothermal Methods

Hydrothermal or solvothermal deposition methods have been applied to modify carbon substrate with small molecules or for polymerization. Different from the typical kinetically driven conditions, hydrothermal reactions are based on the thermodynamic control [148]. During both hydrothermal deposition and polymerization, organic molecules are added to the carbon substrate in an aqueous solution at elevated temperature and pressure [149]. The main advantage is the absence of additional chemical reactant such as oxidizing agent, catalysts or applied electrical energy to drive the reaction. The combined effect of high temperature and pressure provides a one-step process to produce composite electrode materials. Li et al., produced a PEDOT/rGO composite using hydrothermal approach leveraging the oxygen functionalities on the rGO surface as a catalyst for the polymerization. When compared with physically mixed PEDOT, the former exhibited a $1.5\times$ increase in capacitance [148]. Quinone based molecules such as 4-naphthoquinone have also been polymerized on graphene hydrothermally to form flexible electrodes [150]. This method is very versatile and provides the means for simple, scalable and fast production of electrode materials.

3.2.4. Direct Deposition

While polymeric materials are often deposited via electro- or chemical- polymerization, small redox active molecules can be deposited through direct deposition. One way is to modify the carbon substrate and/or the organic molecules with added functionalities such as polar groups [151] or sulfonate groups [118], so that the components can interact via hydrogen bonds, π - π interactions leveraging the sp^2 carbon structure of the substrate, or covalent bonds [118]. The other approach of applying organic compounds to carbon is through electrostatic self-assembly [56,152]. For instance, negatively charged oxygen functional groups on GO or CNT can be used to attract and retain cationic molecules. This simple and effective solution process enables the deposition of monolayers to few layers with good control of the morphology and thickness of the final composite electrodes.

Other techniques that have been explored include vapor phase polymerization (VPP) and oxidative vapor phase polymerization (OVPP) [153]. As an example, Yang and coworkers successfully deposited PEDOT on SWNTs and rGO substrates using VPP [60]. These methods produce thin films of polymer on substrates and have advantages such as

independence of the solubility of monomers, and the possibility of multiple monomers in one reaction chamber for synthesis of copolymers, which are promising for large scale manufacturing of functional and stable composite electrodes [154].

4. Current Advances on Capacitive Organic-Carbon Composite Electrodes

The design and fabrication of redox active organic-carbon composites begins with an understanding of the fundamental interactions between the redox active species and its substrate. Although the main motivation of this review is to introduce a wide range of organic-carbon composites, our survey will start with the well-known CPs (PANI, PPy and PEDOT-PSS) to establish the fundamentals. Using these baselines, we will discuss the promising organic-carbon composites systems. Table 2 lists a series of capacitive CPs-, redox active molecules- and compounds-carbon composite systems, from fabrication, types of bonding, to their performance. The majorities of the carbon substrates in Table 2 are graphene [155] and CNTs, which reflects the current focus in research. Nonetheless, the composites based on organic redox active materials with high surface and low cost ACs are equally important or even more so for commercialization. While the goals of developing composite electrodes are to increase the capacitances and energy densities, power and rate capability for capacitive electrodes are equally important. It is necessary to balance these parameters when designing and processing the capacitive electrodes to avoid developing just “mediocre batteries” [156].

Table 2. Comparison of fabrication methods, bonding type, thickness, and electrochemical performance for some redox active polymers and small molecules deposited on CNT, graphene and activated carbon.

Materials	Fabrication Method	Type of Bonding	Thickness Coating (nm)	Electrolyte	Capacitance	Stability	Ref.
CNT-PANI on GCE	In-situ polymerization	Chemical interaction	10–25	0.5 M H ₂ SO ₄ vs. Ag/AgCl	CV: 354.3 F/g, GCD: 368.4 F/g	-	[157]
AN/SAN-CP (1:1)	Electropolymerization	-	30	1 M H ₂ SO ₄ vs. Ag/AgCl	273.3 F/g (0.5 A/g)	96.1% (5000 cycles, 2 A/g)	[158]
PANI-Graphene	Chemical grafting	Covalent	-	1 M H ₂ SO ₄ vs. Ag/AgCl	482.8 F/g (50 mV/s)	-	[159]
PPy-rGO	Electropolymerization	-	830	1 M H ₂ SO ₄ vs. Ag/AgCl	424 F/g (1 A/g)	-	[160]
PPy-CP-50					13.42 mF/cm ²	51.3% (3 mA/cm ² , 1000 cycles)	
PPy-CP-100	Electropolymerization			1 M H ₂ SO ₄ vs. Ag/AgCl	7.2 mF/cm ²	59.3% (3 mA/cm ² , 1000 cycles)	[161]
PPy-CP-200					3.58 mF/cm ²	63.5% (1000 cycles, 3 mA/cm ²)	
PD4ET-g-GO	Chemical grafting	Covalent	-	1 M KOH vs. Ag/AgCl	561 F/g (5 mV/s)	98% (10,000 cycles, 20 A/g)	[162]
NG/PEDOT	Solution Mixing	π - π stacking	-	1. M H ₂ SO ₄ vs. Ag/AgCl	536 F/g (0.5 A/g)	100% (10,000, 10 A/g)	[163]
poly-p-PD-rGO	Solvothermal	Covalent	-	0.5 M H ₂ SO ₄ vs. SCE	342 F/g (100 mV/s), 347 F/g (0.5 A/g)	90.1% (1000 cycles, 10 A/g)	[164]
poly-o-PD-rGO	Hydrothermal	-	-	2. M H ₂ SO ₄ vs. Ag/AgCl	515 mF/cm ² (1.6 mA/cm ²), 308.3 F/g (1 A/g)	99% (1500 cycles, 1 A/g)	[49]

Table 2. Cont.

Materials	Fabrication Method	Type of Bonding	Thickness Coating (nm)	Electrolyte	Capacitance	Stability	Ref.
poly-o-PD-rGO	In-situ polymerization	Covalent	2–4 (dots)	1. M H ₂ SO ₄ vs. Ag/AgCl	381 F/g (1 A/g)	100% (5000 cycles, 250 mV/s)	[165]
CpF-CNT	Dip coating	π - π stacking	1–2	0.5 M H ₂ SO ₄ vs. Ag/AgCl	30 F/cm ³ (50 mV/s)	95% (5000 cycles, 1 V/s)	[166]
EpF-CNT	Electro-polymerization		1–2		32 F/cm ³ (50 mV/s)		
CpLum-CNT	In-situ polymerization	π - π stacking	4.5	1 M H ₂ SO ₄ vs. Ag/AgCl	48 F/cm ³ (100 mV/s)	95% (4000 cycles, 1 V/s)	[107]
GPDH-rGO	Hydrothermal		-		CV: 316 F/g at 10 mV/s, GCD: 303.88 F/g at 0.5 A/g	93.66% (4000 cycles, 2 A/g)	[151]
		Covalent		2 M H ₂ SO ₄			
GHPD-rGO	Hydrothermal		-		CV: 249 F/g at 10 mV/s, GCD: 231 F/g at 0.5 A/g	87.14% (4000 cycles, 2 A/g)	
o-PD-graphene		π - π stacking	-		367 F/g at 50 mV/s	83% (10,000 cycles, 2 A/g)	
m-PD-graphene	Hydrothermal	Covalent	-	1 M H ₂ SO ₄ vs. Ag/AgCl	372 F/g at 50 mV/s	89% (10,000 cycles, 2 A/g)	[48]
p-PD-graphene			-		473 F/g at 50 mV/s		
p-PD-BC	Solvothermal	Covalent (CO-NH)	4	2 M KOH vs. Hg/HgO	451 F/g at 2 mV/s	92% (5000 cycles, 100 mV/s)	[47]
				1 M H ₂ SO ₄ vs. SCE	442 F/g, 2 mV/s	-	
p-PD-FGA1			-		206 F/g at 10 mV/s	94% (5000 cycles, 250 mV s ⁻¹)	
p-PD-FGA2	Hydrothermal	Covalent bonding		6 M KOH vs. Ag/AgCl	325 F/g at 10 mV/s	-	[167]
p-PD-FGA3					257 F/g at 10 mV/s	98% (5000 cycles, 250 mV s ⁻¹)	
1-pyrenebutyric acid-MWCNT	Electrophoretic deposition	π - π stacking	150	0.5 M Na ₂ SO ₄ vs. Ag/AgCl	125 F/g at 50 mV/s	-	[168]
pyrene-FWCNT		π - π stacking			60 F/g at 1 mV/s	-	
COOH-pyrene-FWCNT	Electro-polymerization	π - π stacking	< 5	EC:DMC with 1 M LiPF ₆ vs. Li/Li+	113 F/g at 1 mV/s		[45]
NH ₂ -pyrene-FWCNT		Electrostatic			210 F/g at 1 mV/s		
Ni-Pc-CNT	-	Covalent (amide), π - π stacking	-	1 M Na ₂ SO ₄ vs. Ag/AgCl	186 mF/cm ² at 138 μ A/cm ²	95% (1000 cycles)	[54]
Ni tetra NH-Pc-MWCNT	Direct mixing 1:1 ratio	π - π stacking	50–100 Nano aggregates	1 M H ₂ SO ₄ SCE	981 \pm 57 F/g at 1 A/g	83% (1500 cycles, 1 mA. cm ⁻²)	[56]

Table 2. Cont.

Materials	Fabrication Method	Type of Bonding	Thickness Coating (nm)	Electrolyte	Capacitance	Stability	Ref.
Nickel Tetra-NH-Pc-CNT	Electro-polymreization	-	100	1 M H ₂ SO ₄ vs. Ag/AgCl	673.2 F/g at 50 mV/s	negligeable (1500 cycles at 10 mA. cm ⁻²)	[55]
Nickel Tetra-NH-Pc-OH-CNT	Electro-polymerization	-			391.6 F/g at 50 mV/s	-	
Co-p-TBIm-Pc-rGO	Electro-polymerization	π - π stacking	-	0.5 M H ₂ SO ₄ vs. Ag/AgCl	25.95 F/g at 5 mV/s	-	[169]
Co-p-TAPBIm-Pc-rGO		π - π stacking	-		34.91 F/g at 5 mV/s	-	
TPPS-CNT	Direct deposition	π - π stacking	1.9	1 M H ₂ SO ₄ vs. Ag/AgCl	26.3 ± 1.3 F/cm ³ , 100 mV/s	97% (10,000 cycles, 1000 mV/s)	[118]
CO _{TTA-DHTA-NH₂} -MWCNT	Solvothermal	Covalent (TTA-DHTA) π - π stacking	3–15	1 M Na ₂ SO ₄ vs. Ag/AgCl	-	96% (1000 cycles)	[84]
V-CNS-GO	Solvothermal	Covalent	13.6 ± 4.2	6 M KOH	160 F/g at 1 A/g	100% (3000 cycles, 10 A g ⁻¹)	[170]

Also in this review, the specific capacitances were cited based-on geometric, areal, or volumetric capacitances from different reports, which often makes the comparison difficult. While gravimetric capacitances are acceptable for comparison at the material level, volumetric or areal capacitance in an EC device are much closer to reality.

4.1. PANI-, PPy- and PEDOT-Carbon Composites

The PANI-carbon composites have been well studied and reported, with various fabrication methods to manipulate the structure, morphology and chemical properties of such composites [22,171–175]. Ordered nanostructures like PANI-CNT core-shell (10–20 nm) yielded greater capacitance compared to the bulk PANI electrodes (Figure 7a, Table 2) [157]. This increase was due to the thinner coating that provided a better utilization of the nitrogen redox center in the polymer. The coverage of the individual nanotubes also led to a smaller diffusion length of the electrolyte ions enabling fast charge/discharge processes. The formation of such core-shell nanocomposite can have increased internal resistance compared to the bare CNT substrate and pure PANI electrodes [157].

Gao et al. investigated the covalent bonding of PANI on rGO substrate by controlled diazotization, where aniline monomers were grafted onto rGO prior to the polymerization. The end result is the formation of PANI nanofiber on the surface, enabling lesser structural changes in the composite during charging/discharging processes [159]. The pipe-like pores in the composite facilitated the diffusion of the electrolyte inside the electrode. The combination of a-Graphene and PANI was enough to increase the overall structural resilience, and improved capacitance of 482.8 F/g compared to 180.3 F/g and 451.5 F/g for rGO and PANI, respectively) (Table 2) [159]. Stability wise, the composite lost about 30% of its initial capacitance after the first 200 cycles and then stabilized, while the decay in pure PANI electrode continued (Figure 7b).

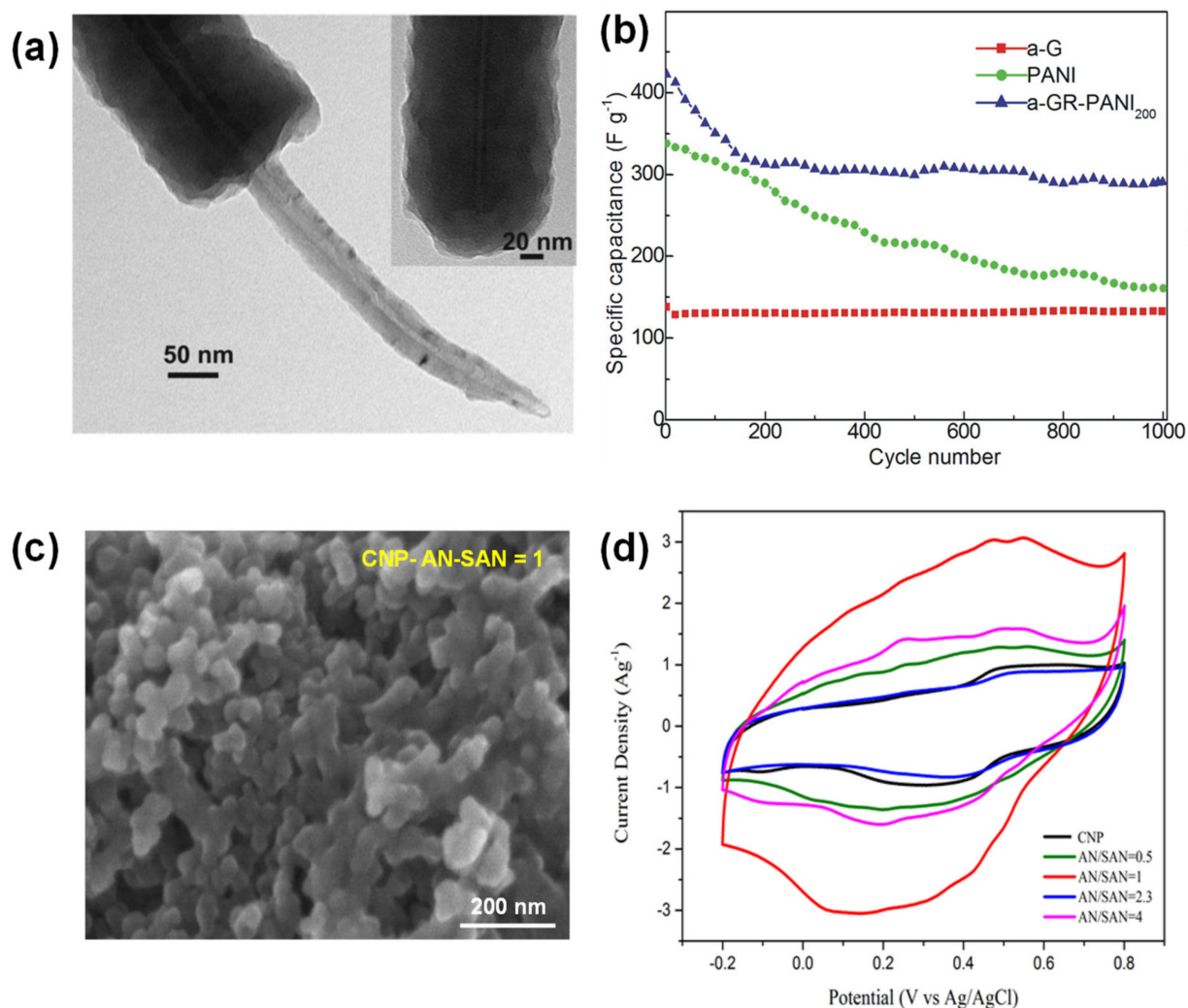


Figure 7. (a) TEM image of PANI-CNT composite, (b) cycling stability of PANI-CNT, (c,d) SEM micrograph of the optimized composite and CV profile comparison of carbon black (CNP) and CNP electrochemically modified with AN/SAN at ratio from 1 to 4. Reproduced with permission from Refs. [157–159].

While PANI has been extensively studied on graphene, AC based substrates present a low-cost alternative. Carbon black nanoparticles (CNP) were modified with PANI self-doped with *o*-aminobenzene sulfonic acid (AN/SAN-CNP) and formed a 30 nm thick coating (Figure 7c). The AN/SAN ratio was optimized to reach the highest current in CV profile at 1:1 (Figure 7d). Further increase in SAN in the composite blocked pores of CNP and decreased the active surface area. This example demonstrated that utilizing monomers with functional groups acting as internal doping agents can help to ease the fabrication of doped PANI composite electrodes without additional purification steps [158]. This also shows that AC based substrate can be coated with thin layers of polymeric material to achieve the desired capacitive performance (Table 2).

Composites based on PPy-carbon tend to have lower gravimetric capacitances and high volumetric capacitance than that of PANI-based composites because of the higher density of PPy, especially with thicker layers [21,176]. The difference is due to the cauliflower-structures in PPy films relative to the nanofibrils of PANI films [21]. While most studies use external chemical doping to increase the conductivity of the PPy, Chang et al. utilized the oxygen group on GO to dope the polymer during the fabrication of the PPy-rGO composite (Figure 8a). This allowed for an improved electronic conductivity and a significantly reduced interfacial resistance as evidenced by impedance measurement (Figure 8b), together with a greater capacitance than the pristine PPy films and PPy-GO (Table 2) [160].

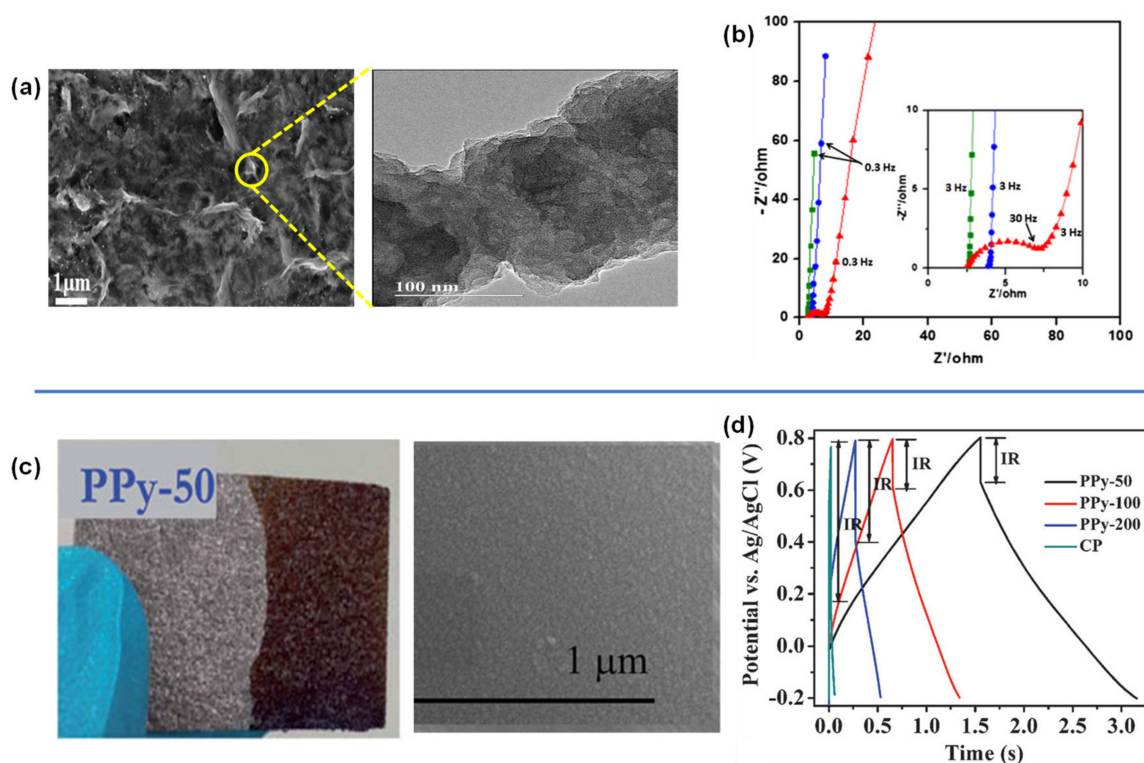


Figure 8. (a,b) Surface morphology and Nyquist plots of rGO modified with PPy, (c) optical and SEM images of PPy deposited on CP at 50 mV/s, and (d) Comparison of GCD curves of carbon paper and PPy-CP fabricated at various scan rates. Reproduced with permission from Refs. [160,161].

PPy composites have also been demonstrated with other carbon substrates. Wei et al. electropolymerized PPy on carbon papers (PPy-CP) using deposition scan rates of 50 mV/s (PPy-50), 100 mV/s (PPy-100), and 200 mV/s (PPy-200) (Figure 8c). A uniform microstructure of the polymer on the carbon paper was obtained with low internal resistance represented by smaller IR drop on the GCD curve for PPy-50 (Figure 8d). This may be the result of the kinetics of the polymerization reaction, where slower scan rates enable more time to complete the reaction. Nonetheless, the long-term stability is still a challenge, as only 50–60% of capacitance was retained after 1000 cycles (Table 2) [161].

Poly(3,4-ethylenedioxythiophene) (PEDOT) possesses a high electrical conductivity in the p-doped state ($300\text{--}500\text{ S cm}^{-1}$), a wide potential window (up to 1.5 V) as well as good chemical and thermal stability [42,177]. Though the specific gravimetric capacitances of PEDOT-based carbon composites are lower than that of PPy and PANI-based carbon composites owing to the higher molecule weight of PEDOT (142 g mol^{-1}), it is possible to achieve greater cycle life stability because of fewer undesirable side reactions [16].

Weak, non-covalent π - π interactions have often been demonstrated between PEDOT-based carbon composites but may lead to lower stability during charge/discharge cycles [137]. Meanwhile, covalent grafting can ensure stability for PEDOT and polythiophenes on carbon. A study used polythiophene bonded to rGO sheets [162] via alkoxy side group provided a uniform interface and created channels for ion movement in the electrode. This contributed to the composite retaining 57.6% of its capacitance from 1 A g^{-1} at 20 A g^{-1} , promising for high-rate capacitive charge storage.

Among PEDOT-based organic composites, PEDOT/PSS is often reported where the polystyrenesulfonate (PSS) polyanion reduces the swelling of the PEDOT during charging and discharging. When PEDOT/PSS is composited with a carbon substrate, it further promotes cycle stability. Teng et al. synthesized PEDOT/PSS-nitrogen-doped graphene composites through a facile flow-assisted self-assembly and produced a free-standing film, with good capacitance (536 F g^{-1} at 0.5 A g^{-1}) [163].

Concerning the dissolution or stability of conducting polymer in the electrolyte, PANI, PPy and PEDOT require protonation within pH 0–3 to be conducting, but remain insoluble in aqueous media. When composited with graphene, the conducting polymers show reduced cycling-induced swelling and structural degradation and do not have clear side reactions [173]. The CPs-carbon composites in this section represent examples of typical capacitive electrodes achieved by a combination of proper design and optimization of various parameters. When developing high performance electrodes, it is important to rationally assemble the right redox layer with the proper substrates to achieve a complementary effect between the two rather than simply following a well-known procedure.

4.2. Redox Active Small Molecule-Carbon Composites

4.2.1. Phenylenediamine

Phenylenediamine (PD) molecules have shown promising capacitive performance on the surface of graphene. They can prevent the re-stacking of the nanosheets by increasing the interlayer spacing and contribute to the charge storage via reversible faradaic reactions. The fabrication techniques have significant influence on the overall electrochemical responses of the composite electrodes. For instance, reducing the oxygen groups of the GO substrate prior to the covalent bonding of p-PD gave different microstructures and lowered the capacitance from 316 F/g to 249 F/g (Table 2). This was explained by the restacking of rGO upon the reduction of the oxygen groups on the surface, limiting the insertion of the p-PD molecules between the nanosheets [151].

The amount of p-PD molecule in the composite also affected the microstructure and the electrochemical response, as evidenced by the functionalised graphene aerogel (FGA) with p-PD via NH-O covalent bond. The addition of moderate amount (2:1) of p-PD in FGA led to increased surface area with high mesoporosity (Figure 9a) and increased capacitance (325 F/g) (Figure 9b, Table 2). However, excessive p-PD in FGA (3:1) led to decreased pore size and pore volume and lower capacitance (257 F/g). A higher concentration of active molecules in a composite may not necessarily provide better charge storage [167].

In a study on the effects of the position of amine on the performance of PD isomers (Figure 9c), Song et.al. observed that the o-, m-, and p-PD bonded differently with the graphene nanosheets [48]. The o-PD isomer preferred both π - π and covalent bonding, while p-PD and m-PD only formed covalent bonds. The p-PD and m-PD isomers resulted in larger inter-space between the graphene sheets of 1.41 nm and 1.3 nm, whereas o-PD had disordered orientation between the nanosheet with inter-space between 0.61 and 0.43 nm (Table 2). This was attributed to both steric effect and the inconsistent deposition of o-PD between the graphene sheets [48].

Small PD molecules are redox active in both acid and alkaline electrolytes. A mesoporous bubble-like carbon (BC) was covalently coated with 4 nm thick p-PD (p-PD-BC) and resulted in ca. three times increased capacitance in both H₂SO₄ acid (442 F/g) and KOH (451 F/g) electrolytes. The composite displayed excellent cycling stability for 5000 cycles in both electrolytes due to the inherent chemical stability of the p-PD molecules and the CO-NH covalent bond between the p-PD and BC substrate preventing the mass loss of the organic layer (Figure 10a–d) [47].

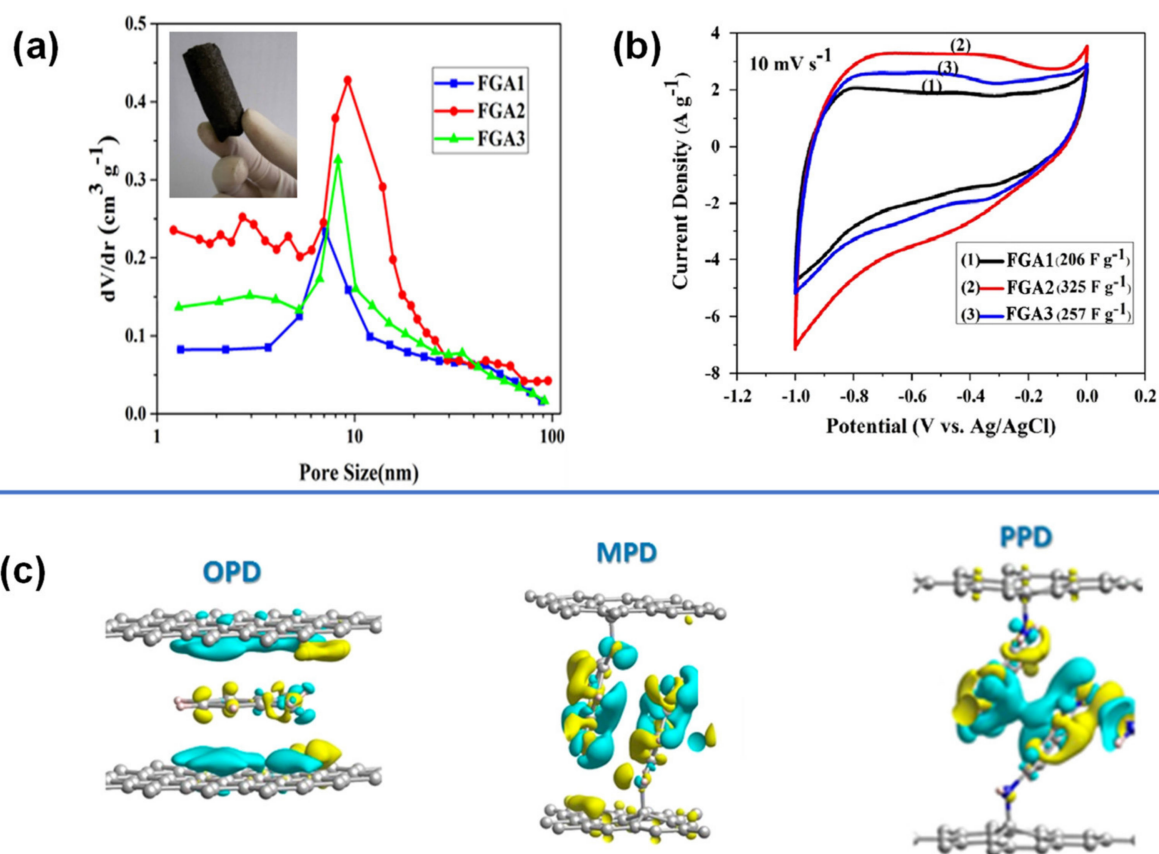


Figure 9. (a,b) Pore size distribution and CV profile at 10 mV/s of p-PD functionalized graphene aerogel (FGA), (c) o, m, p-PD isomers intercalated between graphene sheet Reproduced with permission from Refs. [48,167].

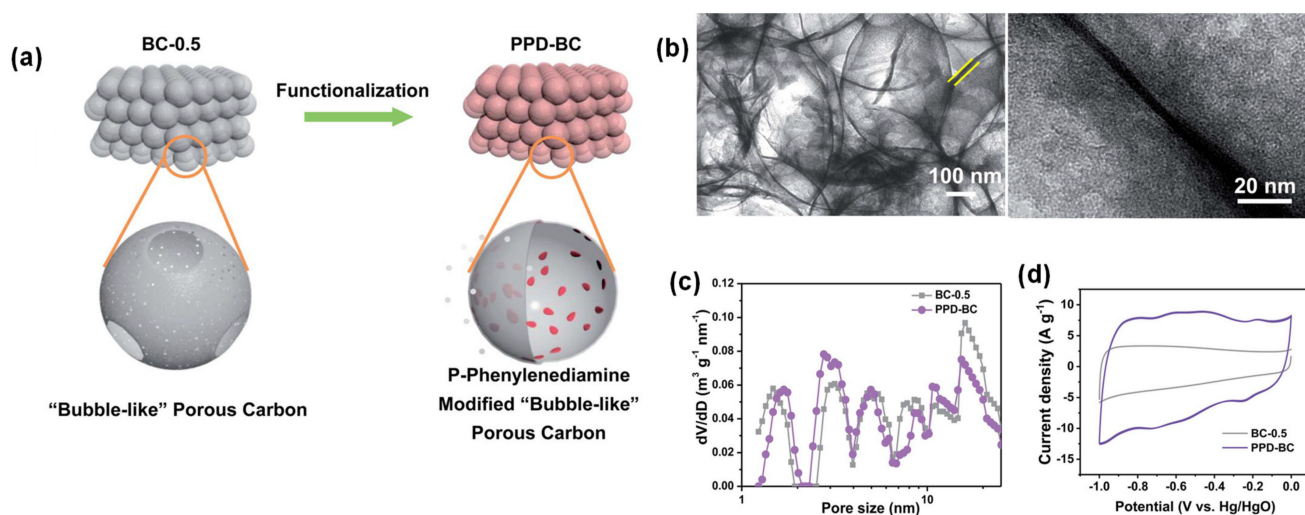


Figure 10. (a–d) fabrication process, morphology, pore size distribution, and CV profile of BC-p-PD composite electrode. Reproduced with permission from Ref. [47].

4.2.2. Macrocycles (Porphyrin/Phthalocyanines)

Chidembo et al. demonstrated an application of porphyrin/phthalocyanine macrocycles for energy storage in 2010 [55,56]. Ni tetra amino-phthalocyanine (NiTAPc) powder was mechanically mixed with CNT in 1:1 ratio to form a composite with nanoaggregates of 50–100 nm. The composite exhibited a large capacitance of $981 \pm 57 \text{ F/g}$ at 1 A/g in $1 \text{ M H}_2\text{SO}_4$ over a potential window of 0.5 V. The enhanced capacitance was attributed to sev-

eral factors: (a) the quinonyl oxygen functionalities on the substrate; (b) electron exchanged from the Ni in the macrocycle; and (c) the imine-like groups within the phthalocyanine. Nonetheless, the composite had a sharp loss in capacitance from about 18 mF/cm^2 in the first hundred cycles to stabilizing at around 14 mF/cm^2 . This decrease was related to the weak interactions between the NiTAPc and CNT [56]. The same author electropolymerized NiTAPc on CNT and reported that the PolyNiTAPc had higher electrochemical response in acidic environment than in alkaline [55] (Table 2). This was explained by the stronger interaction between the nitrogen groups in the phthalocyanine ring and the H_3O^+ from the H_2SO_4 electrolyte. The electropolymerized NiTAPc also had a better capacitance retention after 1500 cycles compared to the mechanically mixed composite in their previous work [56].

A thin layer (1.9 nm) metal-free tetraphenylporphyrin sulfonate was deposited on CNT (Figure 11a). The composite electrode had doubled capacitance over that of bare CNT (Figure 11b, Table 2). The enhanced capacitance was from the synergy between the substrate and the macrocycles, where a 9% decrease in HOMO-LUMO gap for the TPPS molecule was observed. This change in molecular orbital suggest that the kinetics of the charge storage process in the composite is relatively fast and is mostly due to the surface redox processes. In addition, the TPPS-CNT exhibited high cycling stability for 10,000 cycles (Figure 11c) [118].

The presence of substituents on the macrocycle ring affects the overall electrochemical responses of the porphyrin/phthalocyanine molecules. For example, nitrogen containing substituents benzimidazole (BIm) or aminobenzimidazole (ABIm) were attached to a cobalt phthalocyanine (CoPc) that was deposit on rGO (Figure 11d) [169]. Both BIm and ABIm substituents tend to electropolymerize upon applied potential to give poly-BIm and poly-ABIm. The resulting composites had multiple redox peaks in wide potential range from Co central metal atom, pyrrole from Pc ring and pyridinic nitrogen groups from the substituents. The effects of BIm and ABIm substituents on the Pc ring led to different electrochemical behavior. The macrocycle substituted with ABIm forms stable phenazine-like structure once polymerized (Figure 11d). This resulted in a greater capacitance over the Pc substituted with BIm that forms an imine bridges in the polymer (Figure 11e), which are less reactive than their phenazine counterpart (Table 2) [169].

The great advantages of macrocycles are their highly tunable chemical and electronic properties that could be exploited to design their electrochemical behavior. This aspect is promising from synthesis standpoints but still relatively under-developed. While there are more advances in the areas of photovoltaics, some of their synthetic strategies can be applied as well.

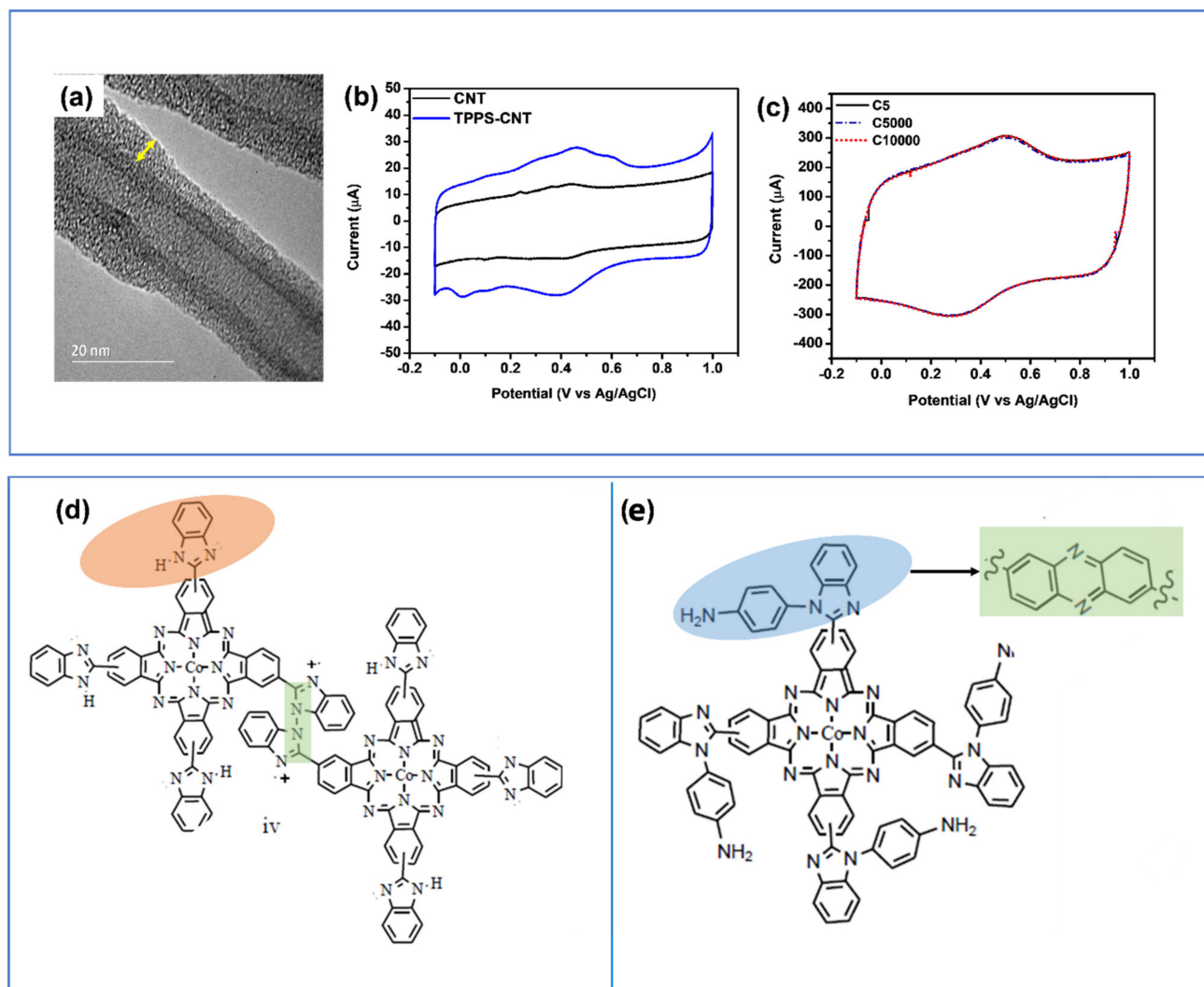


Figure 11. (a–c) TEM image of TPPS-CNT composite electrode with thickness highlighted with yellow arrow, CV profiles comparison of CNT and TPPS-CNT and CV profile of the composite after 5, 5000, and 10,000 cycles, (d,e) Chemical structure of (a) cobalt-poly-tetraaminophenylbenzimidazole phthalocyanine (Co-p-TABim-Pc-rGO) and Co-poly-tetrabenzimidazole (Co-p-TBIm-Pc-rGO). Reproduced with permission from Refs. [118,169].

4.3. Other Polymers

4.3.1. Pyrene Derivatives

Conjugated pyrene derivatives have shown pseudocapacitive characteristics with CNT and graphene. Pyrenes can attach to the carbon substrates by non-covalent (π - π) and covalent bonding [178], whereas the functional groups of COOH -, C=O , and NH_2 add redox features and tend to polymerize upon applied potential [45,168,179]. The π - π bonding is illustrated in Figure 12a, where the pyrene molecules are intercalated between the graphene layers. As a result, the pyrene-graphene composite displayed relatively high conductivity, high stability (Figure 12b,c) and good pseudocapacitive performance. Another example is CNT modified with carboxy (COOH) and amino (NH_2) functionalized pyrene. Electropolymerized COOH -Pyrene and NH_2 -Pyrene exhibited very different redox behavior on oxidized CNT. Although both had reversible redox peaks on their respective CVs, NH_2 -Pyrene-CNT had the most capacitive-like profile. Performance wise, the NH_2 -Pyrene-CNT had nearly twice the capacitance (210 F/g) of COOH -Pyrene-CNT (113 F/g) (Figure 12d,e, Table 2) [45]. Since pyrene derivatives are abundant in industrial waste, applying these molecules in composite electrodes could lead to more sustainability toward lowering the carbon footprints.

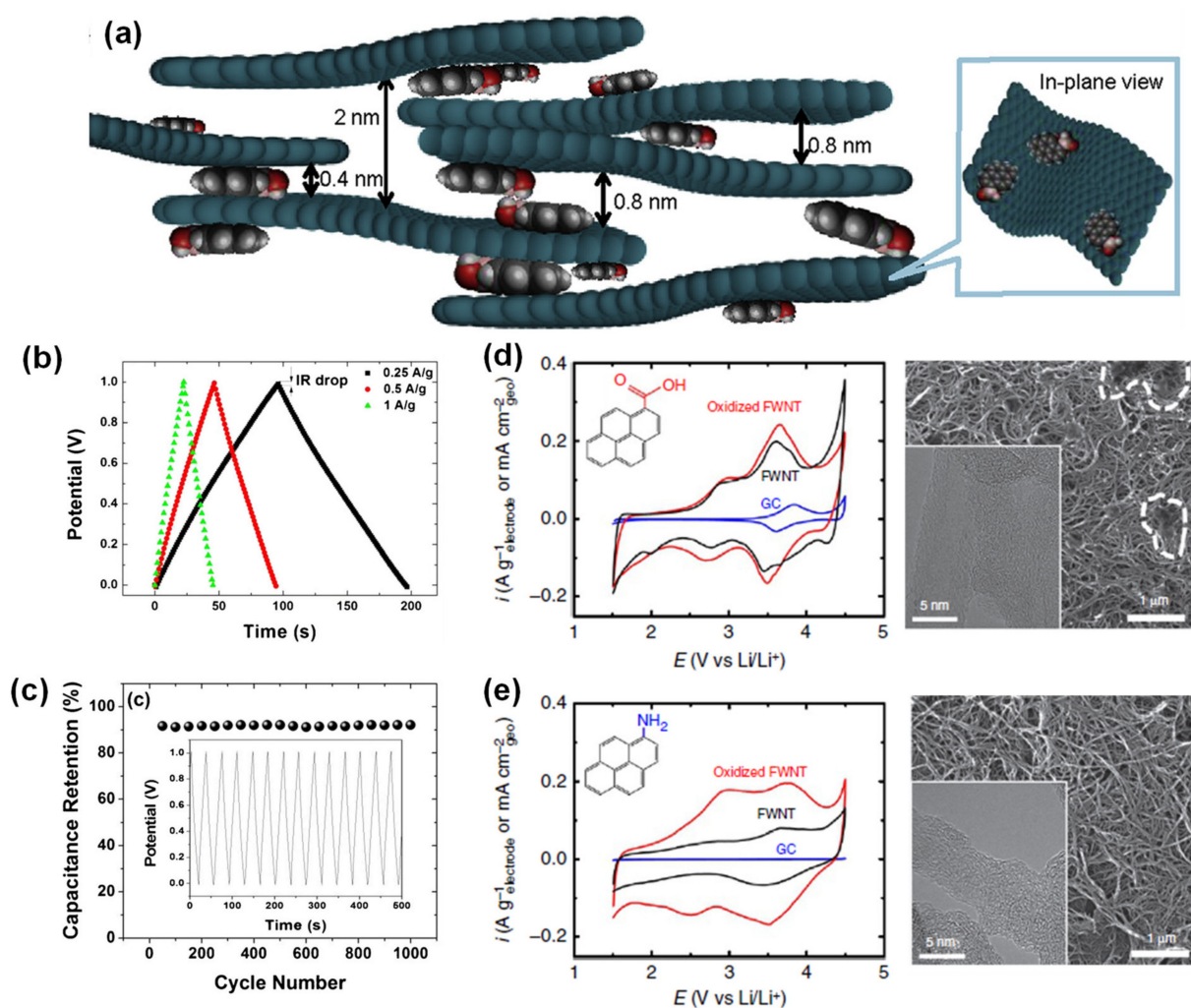


Figure 12. (a) Representation of pyrene intercalated between graphene nanosheets, (b,c) GCD curves at various current density and capacitance retention of the pyrene graphene composite, (d,e) CV profiles of COOH and NH₂-pyrene on FWCNT at 1 mV/s and their corresponding SEM images. Reproduced with permission from Refs. [45,168,180].

4.3.2. Poly-Phenylenediamine

Poly-para-phenylenediamine (poly-p-PD) and poly-ortho-phenylenediamine (poly-o-PD), two isomers of poly-PD covalently attached to rGO substrate formed small polymer dots on the surface (Figure 13a,b). The diameters of the poly-p-PD were 10–50 nm, larger than that of poly-o-PD of 2–4 nm (Figure 13c,d). However, the larger dots on the rGO substrate yielded lower capacitance (Table 2) [49,164,165], reflecting the importance of material utilization: a thin layer and smaller size (in this example) of the active materials on carbonaceous materials will lead to more effective utilization and often faster charge storage kinetics of the composites.

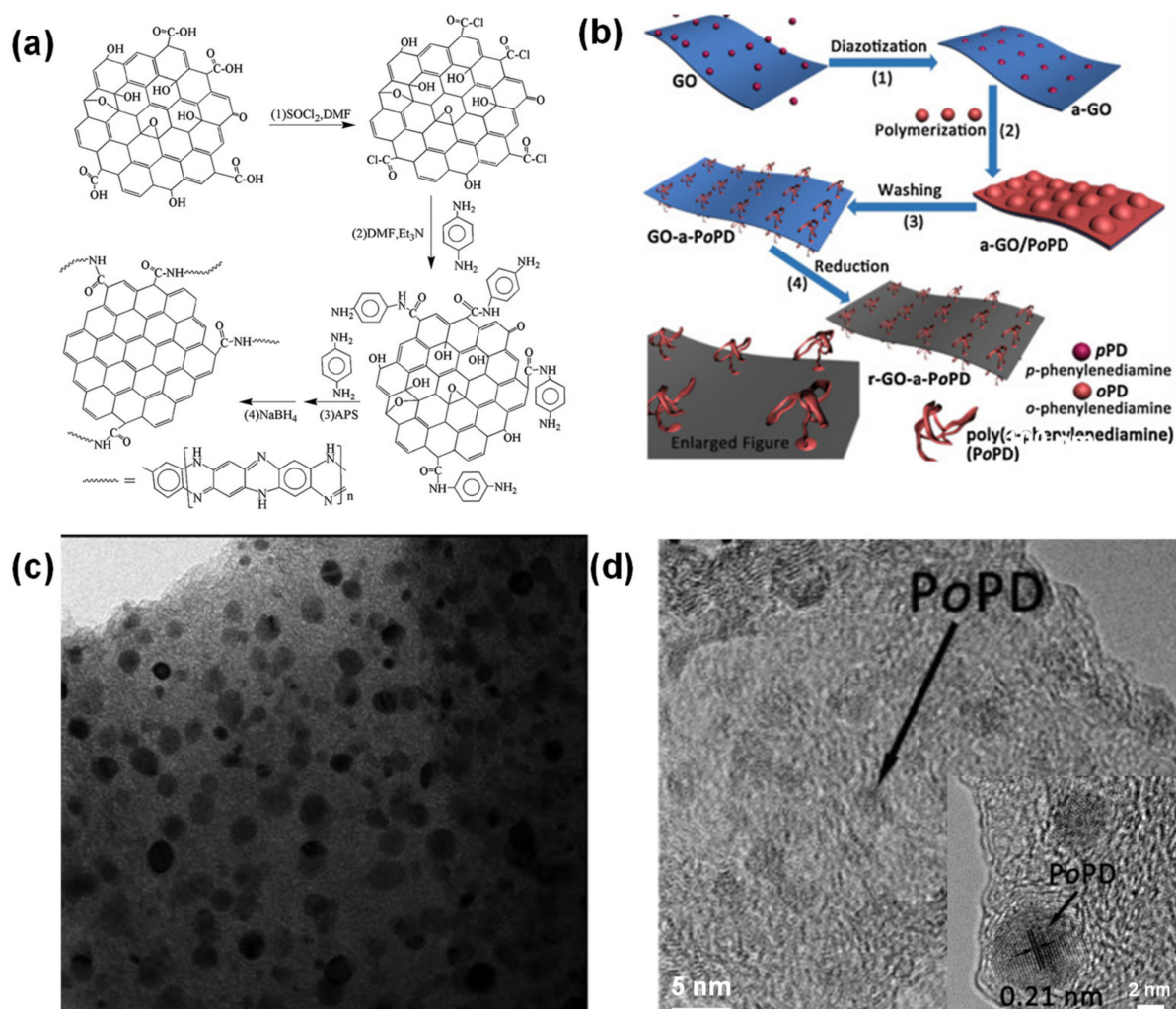


Figure 13. (a,b) Mechanism of the covalent functionalization, and (c,d) HTEM images of rGO modified poly-p-PD and poly-o-PD quantum dots. Reproduced with permission from Refs. [49,164,165].

4.3.3. Polyfuchsin and Polyluminol

Other nitrogen containing polymers such as polyluminol-CNT and polyfuchsin-CNT composites also showed capacitive charge storage properties. N'Diaye et al. demonstrated the polymerization of fuchsin on CNT via both chemical (CpF) and electrochemical (EpF) routes. The composite electrodes exhibited multiple highly reversible faradaic redox reactions, indicative of their pseudocapacitive-like behavior (Figure 14a,b). The enhanced electrochemical performance of the composite electrodes was related to a strong π interaction between the polymers and CNT substrate providing high stability, and the presence of phenazine-like redox groups in the polymeric backbone [166].

A study on chemically polymerized luminol and CNT (CpLum-CNT) revealed that the composite electrodes had c.a. 2.5 times higher volumetric capacitance than that of bare CNT at an optimal 4.5 ± 1.5 nm of polymer (Figure 14c) [107]. Leveraging the quantification method developed by Wang and Dunn [11,27], the capacitive contribution of CpLum-CNT was estimated to be about 74%, with 70% of the total charge stored attributed to CpLum (Figure 14d). It is hypothesized that the electrochemical redox reactions were from the secondary amine (NH) and the amide (NH-C=O) groups in the polymer in comparison to the similar polymers like PANI. However, the actual mechanism needs to be further investigated to differentiate the specific contributions from the multiple functional groups in the polymer.

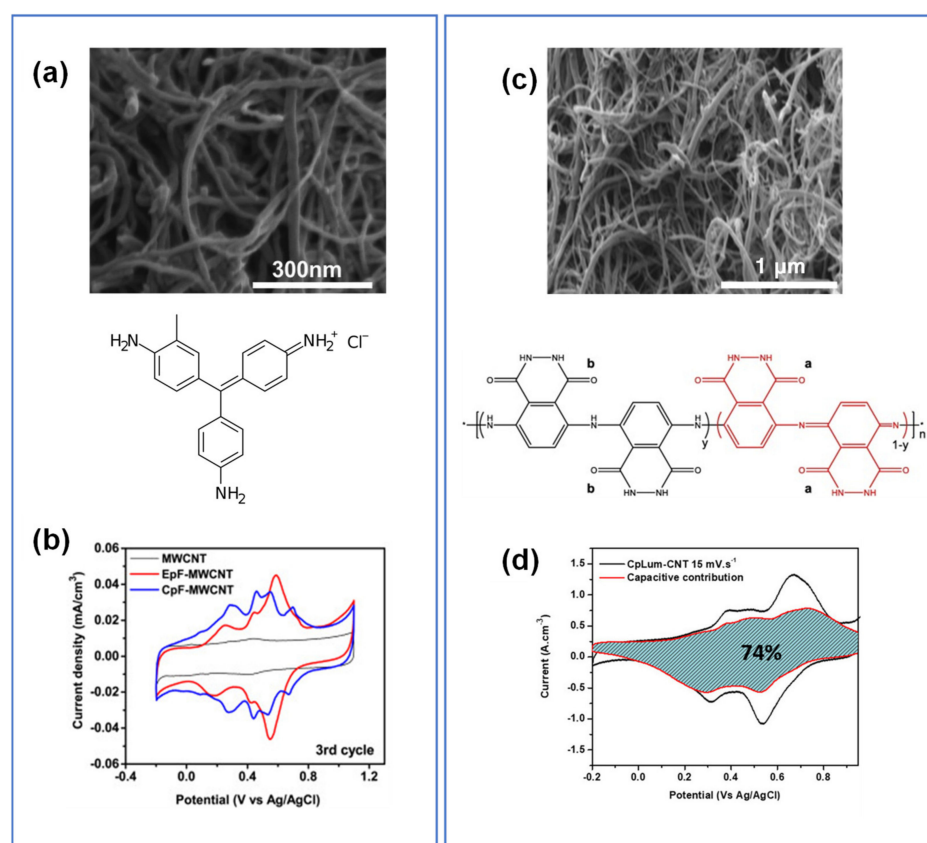


Figure 14. (a,b) SEM, CV profile of CpF-CNT (100 mV/s) and EpF-CNT, (c,d) SEM micrograph and CV profile showing the capacitive contribution in CpLum-CNT composite (15 mV/s). All CVs were obtained in 1 M H₂SO₄ electrolyte. Reproduced with permission from Refs. [107,166].

4.4. Covalent Organic Frameworks (COF)

COFs have been applied directly as electrode materials but suffer from relatively low conductivities [44]. One way to rectify this is through synthesizing composites with electronically conducting carbon materials such as CNTs [84], graphene and GO. Sun et al. used a molecular pillar approach and grew vertical COF nanosheets on GO with covalently bonded diboronic acid (DBA) (Figure 15a,b) acting as the nucleation sites [170]. The resulting vertical nanosheets were 3–15 nm thick with a SSA of up to 700 m²/g (Figure 15c) and capacitance reaching 160 F/g. An alternative route (Figure 15d) to produce platelets parallel to the surface (Figure 15e) showed approximately half the SSA and lower capacitance (90 F/g). This vertical arrangement may have contributed to the stable electrode capacitive behavior over 3000 cycles. Improvements to ion movement have also been achieved with thin layers. Wang et al. synthesized 2D COFs with 4,4',4''-(1,3,5-triazine-2,4,6-triyl)trianiline (TTA) and 2,5-dihydroxyterephthalaldehyde (DHTA) subunits on amino-functionalized MWCNTs using a facile solvothermal method as shown in Figure 15f [84]. The amine-functionalized MWCNT (Figure 15g) with the COF_{TTA-DHTA} shell (Figure 15h) had a thin layer distribution between 12–37 nm, with perpendicularly oriented hexagonal pore channels, promoting ion movement. Furthermore, the customizability of COFs enables efficient and fast proton transfer at hydrophilic sites. Adsorbed water chains transport protons through the removal and formation of O-H bonds via the Grotthuss mechanism, promoting pseudocapacitive behavior [181]. Hence, these structural arrangements and orientations are critical for COFs to be exploited in thin layers in redox active composites. While COF have interesting features, the main challenge is to precisely design these large organic frameworks with redox center that can complement each other to achieve capacitive performance.

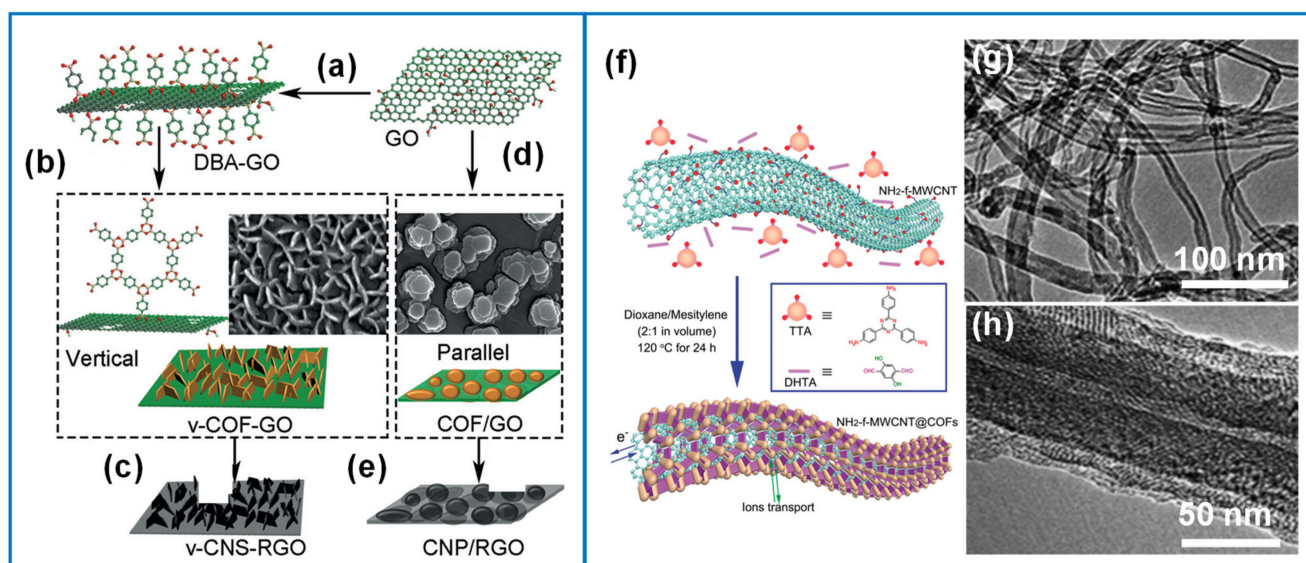


Figure 15. (a) Functionalized GO with DBA in methanol. (b) Vertical COF nanosheets growth using DBA functionalized on GO dissolved in mesitylene/dioxane (*v*-COF-GO). (d) Parallel COF platelets to GO formation without DBA (COF/GO). Carbonization of (c) *v*-COF-GO and (e) COF/GO to produce vertically oriented nanosheets (*v*-CNS-RGO) or parallel to RGO surface (CNP/RGO). (f) Schematic of COFTTA–DHTA shells on the NH₂-f-MWCNT surface. COFTTA–DHTA was constructed from TTA and DHTA via imine linkages. (g) NH₂-f-MWCNT and (h) NH₂-f-MWCNT and COFTTA–DHTA synthesized at 10 mg mL^{−1} of NH₂-f-MWCNT at 120 °C for 24 h. Reproduced with permission from Refs. [84,170].

5. Perspectives and Conclusions

In this review, multiple aspects regarding the development of organic-carbon composites with capacitive charge storage capabilities were discussed. The high-power densities, fast rate, and long charge-discharge life cycles of the capacitive electrodes rely mostly on surface-confined processes, either electrostatic or faradic in nature. While Faradic redox reactions can significantly increase the capacitance and energy storage in organic-carbon composite electrodes, one should consider the surface and interfacial phenomena and try to minimize diffusion limited processes. In addition, for future energy storage solutions, it is also important to take into account the low cost and high environmental sustainability. Below are some suggestions for the future development and improvement of organic-carbon composite electrodes for ECs.

- Organic Materials

The redox active organic compounds and composites should meet the criteria of capacitive nature and have high chemical and electrochemical stability. Pseudocapacitive behavior that shows ideal characteristics as reflected in linear galvanostatic charge-discharge and rectangular voltammograms need to be targeted [177]. Battery-like bulk faradaic behavior, which is not ideal for high-power (rate) capacitive applications but is often reported for supercapacitors, should be differentiated. On the other hand, small molecules, although relatively underexplored, provide more versatile and tunable alternatives to the organic-carbon composites. Recent advancement on fast redox kinetic organic molecules (e.g., a diffusion-free Grotthuss proton-hopping hydrated Prussian blue [182]) and composites has further blurred the boundaries between high-rate battery and high-energy pseudocapacitive materials [3,66,181]. This also makes the organic material synthesis more exciting and challenging with specific performance goals moving forward.

Many redox active species discussed in this review contain either N- or O- functional groups as electrochemical redox centers. Developing novel organic compounds with multiple redox centers could be of interest. A good example would be COFs that could be designed specifically for pseudocapacitance. Recent report on perylene diimide and

hexaazatrinaphthylene system also pointed to a very promising direction to facilitate the diffusion and long-range charge delocalization via molecule contortion [66].

While the redox activity of organic compounds is very appealing for energy storage, researchers should be vigilant to their possible health and environmental issues. The benefits of these organic compounds must significantly outweigh their side effects. The assessments for safety in different conditions and environments is important to determine the proper handling and waste management of these nanomaterials [183].

The electrochemical redox mechanisms of most organic compounds are still based on the consensus from the well-known CPs, with limited evidence connecting to the actual chemical structural changes during the charge/discharge. Efforts are needed to elucidate the redox mechanisms for those electrochemically active compounds using in-situ or operando characterization methods.

- Carbonaceous Substrates

High surface area carbon substrates are ideal for capacitive organic composite electrodes, more particularly those with a rich network of sp^2 hybridizations. Since these contribute to the electric conductivity and bonding, both of which are important for fast and enhanced charge/discharge processes. While CNT and graphene are excellent substrates for fundamental studies of redox active compounds and composites, the cost of these nanomaterials makes them less desirable for large scale productions. Therefore, development efforts should be invested into activated carbon (AC), especially biomass waste derived AC to lessen the environmental impact and further help to meet the target of carbon neutrality. An ideal carbon substrate for bonding with organic molecules needs to have a relatively high conductivity, high surface area with meso sized porosity, high concentrations of sp^2 hybridizations, high surface functional groups to be compatible with the organic layer, and with a simple and low-cost production.

- Computational Aspects

Computational first-principle approaches have shown great promise in predicting the structural and electronic stability of composites based on the interactions of their individual components. Currently, however, studies on composite interactions often do not consider the relationship between the composite components and the electrolyte. This arises from the computational time, cost and complexity of the simulations involved but provides opportunities for further explorations of these aspects. The other area of growing interest is the application of computational design of redox active species for energy storage applications as there is currently a limited number of work demonstrating such molecular design [66,184,185]. Another direction is simulating porous electrodes with their characteristic pores, and surrounding electrolyte environments. Furthermore, accurately modeling solvation behavior of the electrolyte under an electric field provides another route to make computational approaches more applicable [124].

Techniques such as MD can provide good approximations for ion movement and electric double layers but still lack adequately accurate reactive force field potentials for modeling the complex interfacial redox processes for pseudocapacitance [109,186]. This is an important future direction to better predict the interfacial phenomena for redox active composites. For reporting predicted energies, systems with large molecules such as COFs, considerations with respect to the atom count instead of moles should be included to account for the size of the species.

- Design and Fabrication of Composite Electrodes

In this review, various examples of composite electrodes were discussed to demonstrate the importance of proper matching of the individual components in the composite to achieve the desired capacitive charge storage. Below we propose several research directions that could be explored to further push the performance of organic-carbon composites for electrochemical capacitors and beyond.

While the well-known CPs provide insights to the redox pseudocapacitance as well as the interactions with the substrates, high loading with thick bulky CPs to composites

may induce more mass-transfer limited kinetic processes. Research towards optimization and engineering of ideal electrodes is still the key. To achieve this goal, thin layers of active materials should be prioritized over bulkier layers for capacitive charge storage.

In addition to the conventional approaches developing single-layer organic materials, efforts should be directed to leverage the strength of multi-layer of active/functional components to rationally design, tune and optimize the composites. Some redox active organic species do not necessarily have pseudocapacitive-like behavior but still present fast redox kinetics that could be leveraged for ECs. Designing and engineering multi-layer redox active materials to modify the carbon surface may lead to complementary electrochemical contributions to achieve pseudocapacitance and even synergies [187]. It is equally important to develop simple, environmentally friendly and scalable processes that limit the use of harsh chemicals to fabricate composite electrodes. This will be particularly desirable when applying to low-cost materials such as biomass derived AC.

On a more fundamental level, future research should focus on developing in-situ and operando characterization methods to investigate the underlying mechanisms of the redox activity and the interactions between carbon substrate and active materials. While this aspect is relatively less reported, having a deep understanding of the chemical, structural and morphological changes within the composites will enable the development of more efficient and stable composite electrodes for ECs and beyond. Furthermore, the stability of the electrode materials and the occurrence of side reactions should be adequately characterized in future research, by conducting impedance spectroscopy (Nyquist and Bode plots) and cycling tests of at least 5000 to 10,000 cycles.

Although EC devices enabled by capacitive organic-carbon electrodes are not discussed in this review, advanced devices are the destiny for the electrode development. In transition from electrodes to devices, there is a need for design guidelines for ECs (in either liquid- or solid-state). In practice, an electrode with high gravimetric capacitance may not translate to high capacitance in EC devices. A complete EC device not only needs the appropriate electrodes and electrolyte to function but also requires current collectors and packaging. A systematic and comprehensive approach is necessary to identify the optimal matches of electrode chemistries, structures, loadings, and electrolyte interfaces to achieve the ultimate goals of high performing, environmentally safe and low-cost capacitive charge storage solutions.

Author Contributions: J.N.: Writing original draft, Literature collection, Preparation of tables and figures, R.B.: Writing original draft, Literature collection, Preparation of tables and figures, J.Y.H.: writing—review and editing, K.L.: supervision, writing—review and editing. All authors have read and agreed to the published version of the manuscript.

Funding: This research was funded by Natural Sciences and Engineering Research Council of Canada (NSERC) RGPIN-2016-06219 and NFRFE-2019-00739.

Data Availability Statement: Not applicable.

Acknowledgments: Jeanne N'Diaye would like to thank the Hatch graduate scholarship for their financial support.

Conflicts of Interest: The authors declare no conflict of interest.

References

1. Afif, A.; Rahman, S.M.H.; Tasfiah Azad, A.; Zaini, J.; Islan, M.A.; Azad, A.K. Advanced materials and technologies for hybrid supercapacitors for energy storage—A review. *J. Energy Storage* **2019**, *25*, 100852. [[CrossRef](#)]
2. Conway, B.E. *Electrochemical Supercapacitors: Scientific Fundamentals and Technological Applications*; Springer: Boston, MA, USA, 1999; p. 685. [[CrossRef](#)]
3. Simon, P.; Gogotsi, Y. Perspectives for electrochemical capacitors and related devices. *Nat. Mater.* **2020**, *19*, 1151–1163. [[CrossRef](#)] [[PubMed](#)]
4. Simon, P.; Gogotsi, Y. Materials for electrochemical capacitors. *Nat. Mater.* **2008**, *7*, 845–854. [[CrossRef](#)]
5. Fleischmann, S.; Mitchell, J.B.; Wang, R.; Zhan, C.; Jiang, D.E.; Presser, V.; Augustyn, V. Pseudocapacitance: From Fundamental Understanding to High Power Energy Storage Materials. *Chem. Rev.* **2020**, *120*, 6738–6782. [[CrossRef](#)] [[PubMed](#)]

6. Han, Y.; Ge, Y.; Chao, Y.; Wang, C.; Wallace, G.G. Recent progress in 2D materials for flexible supercapacitors. *J. Energy Chem.* **2018**, *27*, 57–72. [[CrossRef](#)]
7. Ke, Q.; Wang, J. Graphene-based materials for supercapacitor electrodes—A review. *J. Mater.* **2016**, *2*, 37–54. [[CrossRef](#)]
8. Conway, B.E. Transition from “Supercapacitor” to “Battery” behavior in electrochemical energy storage. *J. Electrochem. Soc.* **1991**, *138*, 1539–1548. [[CrossRef](#)]
9. Su, F.; Wu, Z.-S. A perspective on graphene for supercapacitors: Current status and future challenges. *J. Energy Chem.* **2021**, *53*, 354–357. [[CrossRef](#)]
10. Wang, J.; Zhang, X.; Li, Z.; Ma, Y.; Ma, L. Recent progress of biomass-derived carbon materials for supercapacitors. *J. Power Sources* **2020**, *451*, 227794. [[CrossRef](#)]
11. Choi, C.; Ashby, D.S.; Butts, D.M.; DeBlock, R.H.; Wei, Q.; Lau, J.; Dunn, B. Achieving high energy density and high power density with pseudocapacitive materials. *Nat. Rev. Mater.* **2020**, *5*, 5–19. [[CrossRef](#)]
12. Kate, R.S.; Khalate, S.A.; Deokate, R.J. Overview of nanostructured metal oxides and pure nickel oxide (NiO) electrodes for supercapacitors: A review. *J. Alloys Compd.* **2018**, *734*, 89–111. [[CrossRef](#)]
13. Low, W.H.; Khiew, P.S.; Lim, S.S.; Siong, C.W.; Ezeigwe, E.R. Recent development of mixed transition metal oxide and graphene/mixed transition metal oxide based hybrid nanostructures for advanced supercapacitors. *J. Alloys Compd.* **2019**, *775*, 1324–1356. [[CrossRef](#)]
14. Mohd Abdah, M.A.A.; Azman, N.H.N.; Kulandaivalu, S.; Sulaiman, Y. Review of the use of transition-metal-oxide and conducting polymer-based fibres for high-performance supercapacitors. *Mater. Des.* **2020**, *186*, 108199. [[CrossRef](#)]
15. Ibanez, J.G.; Rincon, M.E.; Gutierrez-Granados, S.; Chahma, M.; Jaramillo-Quintero, O.A.; Frontana-Uribe, B.A. Conducting Polymers in the Fields of Energy, Environmental Remediation, and Chemical-Chiral Sensors. *Chem. Rev.* **2018**, *118*, 4731–4816. [[CrossRef](#)] [[PubMed](#)]
16. Snook, G.A.; Kao, P.; Best, A.S. Conducting-polymer-based supercapacitor devices and electrodes. *J. Power Sources* **2011**, *196*, 1–12. [[CrossRef](#)]
17. Augustyn, V.; Simon, P.; Dunn, B. Pseudocapacitive oxide materials for high-rate electrochemical energy storage. *Energy Environ. Sci.* **2014**, *7*, 1597–1614. [[CrossRef](#)]
18. Bakker, M.G.; Frazier, R.M.; Burkett, S.; Bara, J.E.; Chopra, N.; Spear, S.; Pan, S.; Xu, C. Perspectives on supercapacitors, pseudocapacitors and batteries. *Nanomater. Energy* **2012**, *1*, 136–158. [[CrossRef](#)]
19. Niu, Z.; Liu, L.; Zhou, W.; Chen, X.; Xie, S. Carbon Nanotube-Based Thin Films for Flexible Supercapacitors. In *Nanocarbons for Advanced Energy Storage*; Wiley-VCH Verlag GmbH & Co. KGaA: Weinheim, Germany, 2015; pp. 279–299. [[CrossRef](#)]
20. Balli, B.; Şavk, A.; Şen, F. Graphene and polymer composites for supercapacitor applications. In *Nanocarbon and Its Composites*; Khan, A., Jawaid, M., Inamuddin Asiri, A.M., Eds.; Woodhead Publishing: Sawston, UK, 2019; pp. 123–151. [[CrossRef](#)]
21. Gao, Y. Graphene and Polymer Composites for Supercapacitor Applications: A Review. *Nanoscale Res. Lett.* **2017**, *12*, 387. [[CrossRef](#)]
22. Magu, T.O.; Agobi, A.U.; Hitler, L.; Dass, P.M. A Review on Conducting Polymers-Based Composites for Energy Storage Application. *J. Chem. Rev.* **2019**, *1*, 19–34.
23. Wu, Q.; Xu, Y.; Yao, Z.; Liu, A.; Shi, G. Supercapacitors based on flexible graphene/polyaniline nanofiber composite films. *ACS Nano* **2010**, *4*, 1963–1970. [[CrossRef](#)] [[PubMed](#)]
24. Noori, A.; El-Kady, M.F.; Rahmanifar, M.S.; Kaner, R.B.; Mousavi, M.F. Towards establishing standard performance metrics for batteries, supercapacitors and beyond. *Chem. Soc. Rev.* **2019**, *48*, 1272–1341. [[CrossRef](#)]
25. Taberna, P.L.; Simon, P.; Fauvarque, J.F. Electrochemical Characteristics and Impedance Spectroscopy Studies of Carbon-Carbon Supercapacitors. *J. Electrochem. Soc.* **2003**, *150*, A292. [[CrossRef](#)]
26. Eftekhari, A. The mechanism of ultrafast supercapacitors. *J. Mater. Chem. A* **2018**, *6*, 2866–2876. [[CrossRef](#)]
27. Wang, J.; Polleux, J.; Lim, J.; Dunn, B. Pseudocapacitive Contributions to Electrochemical Energy Storage in TiO₂(Anatase) Nanoparticles. *J. Phys. Chem. C* **2007**, *111*, 14925–14931. [[CrossRef](#)]
28. Cook, J.B.; Kim, H.-S.; Lin, T.C.; Lai, C.-H.; Dunn, B.; Tolbert, S.H. Pseudocapacitive Charge Storage in Thick Composite MoS₂ Nanocrystal-Based Electrodes. *Adv. Energy Mater.* **2017**, *7*, 1601283. [[CrossRef](#)]
29. Augustyn, V.; White, E.R.; Ko, J.; Grüner, G.; Regan, B.C.; Dunn, B. Lithium-ion storage properties of titanium oxide nanosheets. *Mater. Horiz.* **2014**, *1*, 219–223. [[CrossRef](#)]
30. Le, T.H.; Kim, Y.; Yoon, H. Electrical and Electrochemical Properties of Conducting Polymers. *Polymers* **2017**, *9*, 150. [[CrossRef](#)] [[PubMed](#)]
31. Kar, P. Classification of Dopants for the Conjugated Polymer. *Doping Conjug. Polym.* **2013**, 19–46. [[CrossRef](#)]
32. Kar, P. Role of Dopant on the Conduction of Conjugated Polymer. *Doping Conjug. Polym.* **2013**, 63–79. [[CrossRef](#)]
33. Chen, S.; Zhitomirsky, I. Influence of dopants and carbon nanotubes on polypyrrole electropolymerization and capacitive behavior. *Mater. Lett.* **2013**, *98*, 67–70. [[CrossRef](#)]
34. Kar, P. Doping Techniques for the Conjugated Polymer. *Doping Conjug. Polym.* **2013**, 47–62. [[CrossRef](#)]
35. Bryan, A.M.; Santino, L.M.; Lu, Y.; Acharya, S.; D’Arcy, J.M. Conducting Polymers for Pseudocapacitive Energy Storage. *Chem. Mater.* **2016**, *28*, 5989–5998. [[CrossRef](#)]
36. Cheng, M.; Meng, Y.N.; Wei, Z.X. Conducting Polymer Nanostructures and their Derivatives for Flexible Supercapacitors. *Isr. J. Chem.* **2018**, *58*, 1299–1314. [[CrossRef](#)]

37. Kim, J.; Kim, J.H.; Ariga, K. Redox-Active Polymers for Energy Storage Nanoarchitectonics. *Joule* **2017**, *1*, 739–768. [[CrossRef](#)]
38. Kim, J.; Lee, J.; You, J.; Park, M.-S.; Hossain, M.S.A.; Yamauchi, Y.; Kim, J.H. Conductive polymers for next-generation energy storage systems: Recent progress and new functions. *Mater. Horiz.* **2016**, *3*, 517–535. [[CrossRef](#)]
39. Wang, H.; Lin, J.; Shen, Z.X. Polyaniline (PANi) based electrode materials for energy storage and conversion. *J. Sci. Adv. Mater. Devices* **2016**, *1*, 225–255. [[CrossRef](#)]
40. Li, H.; Wang, J.; Chu, Q.; Wang, Z.; Zhang, F.; Wang, S. Theoretical and experimental specific capacitance of polyaniline in sulfuric acid. *J. Power Sources* **2009**, *190*, 578–586. [[CrossRef](#)]
41. Peng, C.; Hu, D.; Chen, G.Z. Theoretical specific capacitance based on charge storage mechanisms of conducting polymers: Comment on ‘Vertically oriented arrays of polyaniline nanorods and their super electrochemical properties’. *Chem. Commun.* **2011**, *47*, 4105–4107. [[CrossRef](#)]
42. Lota, K.; Khomenko, V.; Frackowiak, E. Capacitance properties of poly(3,4-ethylenedioxythiophene)/carbon nanotubes composites. *J. Phys. Chem. Solids* **2004**, *65*, 295–301. [[CrossRef](#)]
43. Liu, T.; Li, Y. Addressing the Achilles’ heel of pseudocapacitive materials: Long-term stability. *InfoMat* **2020**, *2*, 807–842. [[CrossRef](#)]
44. Li, J.; Jing, X.; Li, Q.; Li, S.; Gao, X.; Feng, X.; Wang, B. Bulk COFs and COF nanosheets for electrochemical energy storage and conversion. *Chem. Soc. Rev.* **2020**, *49*, 3565–3604. [[CrossRef](#)]
45. Bachman, J.C.; Kaviani, R.; Graham, D.J.; Kim, D.Y.; Noda, S.; Nocera, D.G.; Shao-Horn, Y.; Lee, S.W. Electrochemical polymerization of pyrene derivatives on functionalized carbon nanotubes for pseudocapacitive electrodes. *Nat. Commun.* **2015**, *6*, 7040. [[CrossRef](#)]
46. Ghosh, S.; An, X.; Shah, R.; Rawat, D.; Dave, B.; Kar, S.; Talapatra, S. Effect of 1-Pyrene Carboxylic-Acid Functionalization of Graphene on Its Capacitive Energy Storage. *J. Phys. Chem. C* **2012**, *116*, 20688–20693. [[CrossRef](#)]
47. Huangfu, C.; Liu, Z.; Zhou, Q.; Wang, L.; Wei, T.; Qiu, Z.; Zhang, S.; Fan, Z. Covalent grafting of p-phenylenediamine molecules onto a “bubble-like” carbon surface for high performance asymmetric supercapacitors. *J. Mater. Chem. A* **2020**, *8*, 1767–1778. [[CrossRef](#)]
48. Song, B.; Choi, J.I.; Zhu, Y.; Geng, Z.; Zhang, L.; Lin, Z.; Tuan, C.-C.; Moon, K.-S.; Wong, C.-P. Molecular Level Study of Graphene Networks Functionalized with Phenylenediamine Monomers for Supercapacitor Electrodes. *Chem. Mater.* **2016**, *28*, 9110–9121. [[CrossRef](#)]
49. Yadegari, H.; Heli, H.; Jabbari, A. Graphene/poly(ortho-phenylenediamine) nanocomposite material for electrochemical supercapacitor. *J. Solid State Electrochem.* **2013**, *17*, 2203–2212. [[CrossRef](#)]
50. Jaffe, A.; Saldivar Valdes, A.; Karunadasa, H.I. Quinone-Functionalized Carbon Black Cathodes for Lithium Batteries with High Power Densities. *Chem. Mater.* **2015**, *27*, 3568–3571. [[CrossRef](#)]
51. Suematsu, S.; Naoi, K. Quinone-introduced oligomeric supramolecule for supercapacitor. *J. Power Sources* **2001**, *97–98*, 816–818. [[CrossRef](#)]
52. Tabor, D.P.; Gómez-Bombarelli, R.; Tong, L.; Gordon, R.G.; Aziz, M.J.; Aspuru-Guzik, A. Mapping the frontiers of quinone stability in aqueous media: Implications for organic aqueous redox flow batteries. *J. Mater. Chem. A* **2019**, *7*, 12833–12841. [[CrossRef](#)]
53. Gao, P.; Chen, Z.; Zhao-Karger, Z.; Mueller, J.E.; Jung, C.; Klyatskaya, S.; Diemant, T.; Fuhr, O.; Jacob, T.; Behm, R.J.; et al. A Porphyrin Complex as a Self-Conditioned Electrode Material for High-Performance Energy Storage. *Angew. Chem. Int. Ed. Engl.* **2017**, *56*, 10341–10346. [[CrossRef](#)] [[PubMed](#)]
54. Agboola, B.O.; Ozoemena, K.I. Synergistic enhancement of supercapacitance upon integration of nickel (II) octa [(3,5-bis(carboxylate)-phenoxy) phthalocyanine with SWCNT-phenylamine. *J. Power Sources* **2010**, *195*, 3841–3848. [[CrossRef](#)]
55. Chidembo, A.T.; Ozoemena, K.I. Electrochemical Capacitive Behaviour of Multiwalled Carbon Nanotubes Modified with Electropolymeric Films of Nickel Tetraaminophthalocyanine. *Electroanalysis* **2010**, *22*, 2529–2535. [[CrossRef](#)]
56. Chidembo, A.T.; Ozoemena, K.I.; Agboola, B.O.; Gupta, V.; Wildgoose, G.G.; Compton, R.G. Nickel(ii) tetra-aminophthalocyanine modified MWCNTs as potential nanocomposite materials for the development of supercapacitors. *Energy Environ. Sci.* **2010**, *3*, 228–236. [[CrossRef](#)]
57. Navarro-Suárez, A.M.; Carretero-González, J.; Rojo, T.; Armand, M. Poly(quinone-amine)/nanocarbon composite electrodes with enhanced proton storage capacity. *J. Mater. Chem. A* **2017**, *5*, 23292–23298. [[CrossRef](#)]
58. Fan, L.-Z.; Maier, J. High-performance polypyrrole electrode materials for redox supercapacitors. *Electrochem. Commun.* **2006**, *8*, 937–940. [[CrossRef](#)]
59. Pognon, G.; Cougnon, C.; Mayilukila, D.; Belanger, D. Catechol-modified activated carbon prepared by the diazonium chemistry for application as active electrode material in electrochemical capacitor. *ACS Appl. Mater. Interfaces* **2012**, *4*, 3788–3796. [[CrossRef](#)]
60. Yang, Y.; Zhang, L.; Li, S.; Yang, W.; Xu, J.; Jiang, Y.; Wen, J. Electrochemical performance of conducting polymer and its nanocomposites prepared by chemical vapor phase polymerization method. *J. Mater. Sci. Mater. Electron.* **2013**, *24*, 2245–2253. [[CrossRef](#)]
61. Zhang, J.; Zhao, X.S. Conducting Polymers Directly Coated on Reduced Graphene Oxide Sheets as High-Performance Supercapacitor Electrodes. *J. Phys. Chem. C* **2012**, *116*, 5420–5426. [[CrossRef](#)]
62. Dai, G.; Liu, Y.; Niu, Z.; He, P.; Zhao, Y.; Zhang, X.; Zhou, H. The Design of Quaternary Nitrogen Redox Center for High-Performance Organic Battery Materials. *Matter* **2019**, *1*, 945–958. [[CrossRef](#)]

63. Ji, L.; Krummenacher, I.; Friedrich, A.; Lorbach, A.; Haehnel, M.; Edkins, K.; Braunschweig, H.; Marder, T.B. Synthesis, Photophysical, and Electrochemical Properties of Pyrenes Substituted with Donors or Acceptors at the 4- or 4,9-Positions. *J. Org. Chem.* **2018**, *83*, 3599–3606. [[CrossRef](#)] [[PubMed](#)]
64. Aguilar-Martínez, M.; Antonio Bautista-Martínez, J.; Rivera, E. Thermal, Optical, Electrochemical Properties and Conductivity of Pyrene Monomers. *Des. Monomers Polym.* **2008**, *11*, 173–186. [[CrossRef](#)]
65. Dominska, M.; Jackowska, K.; Kryszynski, P.; Blanchard, G.J. Probing interfacial organization in surface monolayers using tethered pyrene. 1. Structural mediation of electron and proton access to adsorbates. *J. Phys. Chem. B* **2005**, *109*, 15812–15821. [[CrossRef](#)] [[PubMed](#)]
66. Russell, J.C.; Posey, V.A.; Gray, J.; May, R.; Reed, D.A.; Zhang, H.; Marbella, L.E.; Steigerwald, M.L.; Yang, Y.; Roy, X.; et al. High-performance organic pseudocapacitors via molecular contortion. *Nat. Mater.* **2021**, *20*, 1136–1141. [[CrossRef](#)]
67. Guo, C.X.; Lei, Y.; Li, C.M. Porphyrin Functionalized Graphene for Sensitive Electrochemical Detection of Ultratrace Explosives. *Electroanalysis* **2011**, *23*, 885–893. [[CrossRef](#)]
68. Ishihara, S.; Labuta, J.; Van Rossom, W.; Ishikawa, D.; Minami, K.; Hill, J.P.; Ariga, K. Porphyrin-based sensor nanoarchitectonics in diverse physical detection modes. *Phys. Chem. Chem. Phys.* **2014**, *16*, 9713–9746. [[CrossRef](#)] [[PubMed](#)]
69. Lee, C.W.; Lu, H.P.; Lan, C.M.; Huang, Y.L.; Liang, Y.R.; Yen, W.N.; Liu, Y.C.; Lin, Y.S.; Diao, E.W.; Yeh, C.Y. Novel zinc porphyrin sensitizers for dye-sensitized solar cells: Synthesis and spectral, electrochemical, and photovoltaic properties. *Chemistry* **2009**, *15*, 1403–1412. [[CrossRef](#)]
70. Schlettwein, D.; Jaeger, N.I.; Oekermann, T. Photoelectrochemical Reactions at Phthalocyanine Electrodes. In *The Porphyrin Handbook*; Smith, K.M., Guillard, R., Eds.; Academic Press: Amsterdam, The Netherlands, 2003; pp. 247–283. [[CrossRef](#)]
71. Tanaka, T.; Osuka, A. Conjugated porphyrin arrays: Synthesis, properties and applications for functional materials. *Chem. Soc. Rev.* **2015**, *44*, 943–969. [[CrossRef](#)] [[PubMed](#)]
72. Tu, W.; Lei, J.; Ju, H. Noncovalent nanoassembly of porphyrin on single-walled carbon nanotubes for electrocatalytic reduction of nitric oxide and oxygen. *Electrochem. Commun.* **2008**, *10*, 766–769. [[CrossRef](#)]
73. Wang, C.-L.; Lan, C.-M.; Hong, S.-H.; Wang, Y.-F.; Pan, T.-Y.; Chang, C.-W.; Kuo, H.-H.; Kuo, M.-Y.; Diao, E.W.-G.; Lin, C.-Y. Enveloping porphyrins for efficient dye-sensitized solar cells. *Energy Environ. Sci.* **2012**, *5*, 6933–6940. [[CrossRef](#)]
74. Zhou, Q.; Li, C.M.; Li, J.; Cui, X.; Gervasio, D. Template-Synthesized Cobalt Porphyrin/Polypyrrole Nanocomposite and Its Electrocatalysis for Oxygen Reduction in Neutral Medium. *J. Phys. Chem. C* **2007**, *111*, 11216–11222. [[CrossRef](#)]
75. Arıcı, M.; Arıcan, D.; Uğur, A.L.; Erdoğmuş, A.; Koca, A. Electrochemical and spectroelectrochemical characterization of newly synthesized manganese, cobalt, iron and copper phthalocyanines. *Electrochim. Acta* **2013**, *87*, 554–566. [[CrossRef](#)]
76. Liao, M.-S.; Scheiner, S. Electronic structure and bonding in metal porphyrins, metal=Fe, Co, Ni, Cu, Zn. *J. Chem. Phys.* **2002**, *117*, 205–219. [[CrossRef](#)]
77. Koca, A. Spectroelectrochemistry of Phthalocyanines. In *Electrochemistry of N4 Macrocyclic Metal Complexes*; Zagal, J.H., Bedioui, F., Eds.; Springer International Publishing: Cham, Switzerland, 2016; pp. 135–200. [[CrossRef](#)]
78. Castro-Cruz, H.M.; Arias-Aranda, L.R.; Farfán, N.; Xochitlotzi-Flores, E.; Macías-Ruvalcaba, N.A. Elucidating the Electroreduction Mechanism of the Monoprotonated Octaethylporphyrin. A Comparative Study with the Diprotonated Octaethyl- and meso-Tetraphenyl-porphyrins. *J. Electrochem. Soc.* **2020**, *167*, 155507. [[CrossRef](#)]
79. Su, B.; Li, F.; Partovi-Nia, R.; Gros, C.; Barbe, J.-M.; Samec, Z.; Girault, H.H. Evidence of tetraphenylporphyrin monoacids by ion-transfer voltammetry at polarized liquid|liquid interfaces. *Chem. Commun.* **2008**, 5037–5038. [[CrossRef](#)]
80. Langhus, D.L.; Wilson, G.S. Spectroelectrochemistry and cyclic voltammetry of the EE mechanism in a porphyrin diacid reduction. *Anal. Chem.* **1979**, *51*, 1139–1144. [[CrossRef](#)]
81. Mohammed, A.K.; Vijayakumar, V.; Halder, A.; Ghosh, M.; Addicoat, M.; Bansode, U.; Kurungot, S.; Banerjee, R. Weak Intermolecular Interactions in Covalent Organic Framework-Carbon Nanofiber Based Crystalline yet Flexible Devices. *ACS Appl. Mater. Interfaces* **2019**, *11*, 30828–30837. [[CrossRef](#)] [[PubMed](#)]
82. Guan, X.; Chen, F.; Fang, Q.; Qiu, S. Design and applications of three dimensional covalent organic frameworks. *Chem. Soc. Rev.* **2020**, *49*, 1357–1384. [[CrossRef](#)] [[PubMed](#)]
83. Le Comte, A.; Brousse, T.; Bélanger, D. Simpler and greener grafting method for improving the stability of anthraquinone-modified carbon electrode in alkaline media. *Electrochim. Acta* **2014**, *137*, 447–453. [[CrossRef](#)]
84. Sun, B.; Liu, J.; Cao, A.; Song, W.; Wang, D. Interfacial synthesis of ordered and stable covalent organic frameworks on amino-functionalized carbon nanotubes with enhanced electrochemical performance. *Chem. Commun.* **2017**, *53*, 6303–6306. [[CrossRef](#)]
85. Béguin, F.; Presser, V.; Balducci, A.; Frackowiak, E. Carbons and Electrolytes for Advanced Supercapacitors. *Adv. Mater.* **2014**, *26*, 2219–2251. [[CrossRef](#)]
86. Gu, W.; Yushin, G. Review of nanostructured carbon materials for electrochemical capacitor applications: Advantages and limitations of activated carbon, carbide-derived carbon, zeolite-templated carbon, carbon aerogels, carbon nanotubes, onion-like carbon, and graphene. *Wiley Interdiscip. Rev. Energy Environ.* **2014**, *3*, 424–473. [[CrossRef](#)]
87. Hao, L.; Li, X.; Zhi, L. Carbonaceous Electrode Materials for Supercapacitors. *Adv. Mater.* **2013**, *25*, 3899–3904. [[CrossRef](#)] [[PubMed](#)]
88. Lv, W.; Li, Z.; Deng, Y.; Yang, Q.-H.; Kang, F. Graphene-based materials for electrochemical energy storage devices: Opportunities and challenges. *Energy Storage* **2016**, *2*, 107–138. [[CrossRef](#)]

89. Shao, Y.; El-Kady, M.F.; Wang, L.J.; Zhang, Q.; Li, Y.; Wang, H.; Mousavi, M.F.; Kaner, R.B. Graphene-based materials for flexible supercapacitors. *Chem. Soc. Rev.* **2015**, *44*, 3639–3665. [[CrossRef](#)] [[PubMed](#)]
90. Zhang, L.L.; Zhao, X.S. Carbon-based materials as supercapacitor electrodes. *Chem. Soc. Rev.* **2009**, *38*, 2520–2531. [[CrossRef](#)]
91. Miao, L.; Song, Z.; Zhu, D.; Li, L.; Gan, L.; Liu, M. Recent advances in carbon-based supercapacitors. *Mater. Adv.* **2020**, *1*, 945–966. [[CrossRef](#)]
92. Wang, J.-G.; Liu, H.; Zhang, X.; Shao, M.; Wei, B. Elaborate construction of N/S-co-doped carbon nanobowls for ultrahigh-power supercapacitors. *J. Mater. Chem. A* **2018**, *6*, 17653–17661. [[CrossRef](#)]
93. Yang, L.; Wu, D.; Wang, T.; Jia, D. B/N-Codoped Carbon Nanosheets Derived from the Self-Assembly of Chitosan–Amino Acid Gels for Greatly Improved Supercapacitor Performances. *ACS Appl. Mater. Interfaces* **2020**, *12*, 18692–18704. [[CrossRef](#)]
94. Tanguy, N.R.; N'Diaye, J.; Arjmand, M.; Lian, K.; Yan, N. Facile one-pot synthesis of water-dispersible phosphate functionalized reduced graphene oxide toward high-performance energy storage devices. *Chem. Commun.* **2020**, *56*, 1373–1376. [[CrossRef](#)]
95. Xu, C.; Xu, B.; Gu, Y.; Xiong, Z.; Sun, J.; Zhao, X.S. Graphene-based electrodes for electrochemical energy storage. *Energy Environ. Sci.* **2013**, *6*, 1388–1414. [[CrossRef](#)]
96. Tan, Y.B.; Lee, J.-M. Graphene for supercapacitor applications. *J. Mater. Chem. A* **2013**, *1*, 14814–14843. [[CrossRef](#)]
97. Sun, Y.; Shi, G. Self-Assembly of Graphene for Electrochemical Capacitors. In *Nanocarbons for Advanced Energy Storage*; Wiley-VCH Verlag GmbH & Co. KGaA: Weinheim, Germany, 2015. [[CrossRef](#)]
98. Tan, Z.; Chen, G.; Zhu, Y. Carbon-Based Supercapacitors Produced by the Activation of Graphene. In *Nanocarbons for Advanced Energy Storage*; Wiley-VCH Verlag GmbH & Co. KGaA: Weinheim, Germany, 2015; pp. 211–225. [[CrossRef](#)]
99. Brisebois, P.P.; Sijaj, M. Harvesting graphene oxide—Years 1859 to 2019: A review of its structure, synthesis, properties and exfoliation. *J. Mater. Chem. C* **2020**, *8*, 1517–1547. [[CrossRef](#)]
100. Yang, Z.; Tian, J.; Yin, Z.; Cui, C.; Qian, W.; Wei, F. Carbon nanotube- and graphene-based nanomaterials and applications in high-voltage supercapacitor: A review. *Carbon* **2019**, *141*, 467–480. [[CrossRef](#)]
101. Genovese, M.; Lian, K. Polyoxometalate modified pine cone biochar carbon for supercapacitor electrodes. *J. Mater. Chem. A* **2017**, *5*, 3939–3947. [[CrossRef](#)]
102. Genovese, M.; Wu, H.; Virya, A.; Li, J.; Shen, P.; Lian, K. Ultrathin all-solid-state supercapacitor devices based on chitosan activated carbon electrodes and polymer electrolytes. *Electrochim. Acta* **2018**, *273*, 392–401. [[CrossRef](#)]
103. Pandolfo, A.G.; Hollenkamp, A.F. Carbon properties and their role in supercapacitors. *J. Power Sources* **2006**, *157*, 11–27. [[CrossRef](#)]
104. Weinstein, L.; Dash, R. Supercapacitor carbons. *Mater. Today* **2013**, *16*, 356–357. [[CrossRef](#)]
105. Paraknowitsch, J.P.; Thomas, A. Doping carbons beyond nitrogen: An overview of advanced heteroatom doped carbons with boron, sulphur and phosphorus for energy applications. *Energy Environ. Sci.* **2013**, *6*, 2839–2855. [[CrossRef](#)]
106. Kharisov, B.I.; Kharissova, O.V. General Data on Carbon Allotropes. In *Carbon Allotropes: Metal-Complex Chemistry, Properties and Applications*; Kharisov, B.I., Kharissova, O.V., Eds.; Springer International Publishing: Cham, Switzerland, 2019; pp. 1–8. [[CrossRef](#)]
107. N'Diaye, J.; Hyun Chang, J.; Lian, K. The Capacitive Behavior of Polyluminol on Carbon Nanotubes Electrodes. *ChemElectroChem* **2019**, *6*, 5454–5461. [[CrossRef](#)]
108. Wu, H.; Genovese, M.; Ton, K.; Lian, K. A Comparative Study of Activated Carbons from Liquid to Solid Polymer Electrolytes for Electrochemical Capacitors. *J. Electrochem. Soc.* **2019**, *166*, A821–A828. [[CrossRef](#)]
109. Zhan, C.; Lian, C.; Zhang, Y.; Thompson, M.W.; Xie, Y.; Wu, J.; Kent, P.R.C.; Cummings, P.T.; Jiang, D.E.; Wesolowski, D.J. Computational Insights into Materials and Interfaces for Capacitive Energy Storage. *Adv. Sci. (Weinh.)* **2017**, *4*, 1700059. [[CrossRef](#)]
110. Georgakilas, V.; Tiwari, J.N.; Kemp, K.C.; Perman, J.A.; Bourlinos, A.B.; Kim, K.S.; Zboril, R. Noncovalent Functionalization of Graphene and Graphene Oxide for Energy Materials, Biosensing, Catalytic, and Biomedical Applications. *Chem. Rev.* **2016**, *116*, 5464–5519. [[CrossRef](#)]
111. Raimondo, M.; Naddeo, C.; Vertuccio, L.; Bonnaud, L.; Dubois, P.; Binder, W.H.; Sorrentino, A.; Guadagno, L. Multifunctionality of structural nanohybrids: The crucial role of carbon nanotube covalent and non-covalent functionalization in enabling high thermal, mechanical and self-healing performance. *Nanotechnology* **2020**, *31*, 225708. [[CrossRef](#)]
112. Cho, Y.; Cho, W.J.; Youn, I.S.; Lee, G.; Singh, N.J.; Kim, K.S. Density functional theory based study of molecular interactions, recognition, engineering, and quantum transport in π molecular systems. *Acc. Chem. Res.* **2014**, *47*, 3321–3330. [[CrossRef](#)]
113. Jonathan, W. *Steed, J.L.A. Supramolecular Chemistry*, 2nd ed.; Wiley: Hoboken, NJ, USA, 2013.
114. Sholl, D.S.; Steckel, J.A. *Density Functional Theory*; John Wiley & Sons, Inc.: Hoboken, NJ, USA, 2009; pp. 1–238. [[CrossRef](#)]
115. Lazar, P.; Karlický, F.; Jurecka, P.; Kocman, M.; Otyepková, E.; Šafářová, K.; Otyepka, M. Adsorption of small organic molecules on graphene. *J. Am. Chem. Soc.* **2013**, *135*, 6372–6377. [[CrossRef](#)]
116. Mollenhauer, D.; Brieger, C.; Voloshina, E.; Paulus, B. Performance of dispersion-corrected DFT for the weak interaction between aromatic molecules and extended carbon-based systems. *J. Phys. Chem. C* **2015**, *119*, 1898–1904. [[CrossRef](#)]
117. Duan, Y.; Liu, J.; Zhang, Y.; Wang, T. First-principles calculations of graphene-based polyaniline nano-hybrids for insight of electromagnetic properties and electronic structures. *RSC Adv.* **2016**, *6*, 73915–73923. [[CrossRef](#)]
118. N'Diaye, J.; Elshazly, M.; Lian, K. Capacitive Charge Storage of Tetraphenylporphyrin Sulfonate- CNT Composite Electrodes. *Electrochim. Acta* **2021**, *389*, 138593 [[CrossRef](#)]

119. Ahn, D.H.; Park, C.; Song, J.W. Predicting whether aromatic molecules would prefer to enter a carbon nanotube: A density functional theory study. *J. Comput. Chem.* **2020**, *41*, 1261–1270 [[CrossRef](#)] [[PubMed](#)]
120. Kim, H.-J.; Han, Y.-K. How can we describe the adsorption of quinones on activated carbon surfaces? *Curr. Appl. Phys.* **2016**, *16*, 1437–1441. [[CrossRef](#)]
121. Mousavi-Khoshdel, M.; Targholi, E.; Momeni, M.J. First-Principles Calculation of Quantum Capacitance of Codoped Graphenes as Supercapacitor Electrodes. *J. Phys. Chem. C* **2015**, *119*, 26290–26295. [[CrossRef](#)]
122. Özkaya, S.; Blaisten-Barojas, E. Polypyrrole on graphene: A density functional theory study. *Surf. Sci.* **2018**, *674*, 1–5. [[CrossRef](#)]
123. Pykal, M.; Jurečka, P.; Karlický, F.; Otyepka, M. Modelling of graphene functionalization. *Phys. Chem. Chem. Phys.* **2016**, *18*, 6351–6372. [[CrossRef](#)]
124. Ravikumar, B.; Mynam, M.; Rai, B. Molecular dynamics investigation of electric field altered behavior of lithium ion battery electrolytes. *J. Mol. Liq.* **2020**, *300*, 112252. [[CrossRef](#)]
125. Rissanou, A.N.; Harmandaris, V. A molecular dynamics study of polymer/graphene nanocomposites. *Macromol. Symp.* **2013**, *331–332*, 43–49. [[CrossRef](#)]
126. Yang, M.; Koutsos, V.; Zaiser, M. Interactions between polymers and carbon nanotubes: A molecular dynamics study. *J. Phys. Chem. B* **2005**, *109*, 10009–10014. [[CrossRef](#)] [[PubMed](#)]
127. Senftle, T.P.; Hong, S.; Islam, M.M.; Kylasa, S.B.; Zheng, Y.; Shin, Y.K.; Junkermeier, C.; Engel-Herbert, R.; Janik, M.J.; Aktulga, H.M.; et al. The ReaxFF reactive force-field: Development, applications and future directions. *NPJ Comput. Mater.* **2016**, *2*, 15011. [[CrossRef](#)]
128. Elbaz, Y.; Furman, D.; Caspary Toroker, M. Modeling Diffusion in Functional Materials: From Density Functional Theory to Artificial Intelligence. *Adv. Funct. Mater.* **2020**, *30*, 1–18. [[CrossRef](#)]
129. Benda, R.; Zucchi, G.; Cancès, E.; Lebental, B. Insights into the π - π interaction driven non-covalent functionalization of carbon nanotubes of various diameters by conjugated fluorene and carbazole copolymers. *J. Chem. Phys.* **2020**, *152*, 064708. [[CrossRef](#)] [[PubMed](#)]
130. Wang, W.; Zhang, Y.; Liu, W. Bioinspired fabrication of high strength hydrogels from non-covalent interactions. *Prog. Polym. Sci.* **2017**, *71*, 1–25. [[CrossRef](#)]
131. Boukhvalov, D.W. DFT modeling of the covalent functionalization of graphene: From ideal to realistic models. *RSC Adv.* **2013**, *3*, 7150–7159. [[CrossRef](#)]
132. Berisha, A. Interactions between the aryldiazonium cations and graphene oxide: A DFT study. *J. Chem.* **2019**, *2019*, 1–5. [[CrossRef](#)]
133. Oliveira, O.N.; Aoki, P.H.B.; Pavinatto, F.J.; Constantino, C.J.L. Controlled Architectures in LbL Films for Sensing and Biosensing. In *Multilayer Thin Films*; Wiley-VCH Verlag GmbH & Co. KGaA: Weinheim, Germany, 2012; pp. 951–983. [[CrossRef](#)]
134. Mokhtari, A.; Harismah, K.; Mirzaei, M. Covalent addition of chitosan to graphene sheets: Density functional theory explorations of quadrupole coupling constants. *Superlattices Microstruct.* **2015**, *88*, 56–61. [[CrossRef](#)]
135. Gabe, A.; Mostazo-López, M.J.; Salinas-Torres, D.; Morallón, E.; Cazorla-Amorós, D. Synthesis of conducting polymer/carbon material composites and their application in electrical energy storage. In *Hybrid Polymer Composite Materials*; Thakur, V.K., Thakur, M.K., Gupta, R.K., Eds.; Woodhead Publishing: Sawston, UK, 2017; pp. 173–209. [[CrossRef](#)]
136. Zhu, D.; Mo, D.; Ma, X.; Zhou, Q.; Liu, H.; Xu, J.; Zhou, W.; Zhao, F. Effect of polymerization solvent, potential, and temperature on morphology and capacitance properties of poly(thieno[3,2-b]thiophene) films. *Synth. Met.* **2016**, *220*, 155–161. [[CrossRef](#)]
137. Nabilah Azman, N.H.; Lim, H.N.; Sulaiman, Y. Effect of electropolymerization potential on the preparation of PEDOT/graphene oxide hybrid material for supercapacitor application. *Electrochim. Acta* **2016**, *188*, 785–792. [[CrossRef](#)]
138. Zhang, Y.; Zhang, H.; Jiang, F.; Zhou, W.; Wang, R.; Xu, J.; Duan, X.; Wu, Y.; Ding, Y. Electrochemical assembly of homogenized poly(3,4-ethylenedioxythiophene methanol)/SWCNT nano-networks and their high performances for supercapacitor electrodes. *Ionics* **2020**, *26*, 3631–3642. [[CrossRef](#)]
139. Branzoi, F.; Branzoi, V.; Musina, A. Coatings based on conducting polymers and functionalized carbon nanotubes obtained by electropolymerization. *Prog. Org. Coat.* **2013**, *76*, 632–638. [[CrossRef](#)]
140. Si, K.; Guo, X.Q.; Qiu, K.Y. Initiation Mechanism of Radical Polymerization Using Ammonium Persulfate and Polymerizable Amine Redox Initiators. *J. Macromol. Sci. Part A* **1995**, *32*, 1149–1159. [[CrossRef](#)]
141. Mart, H. Oxidative polycondensation reaction. *Des. Monomers Polym.* **2012**, *9*, 551–588. [[CrossRef](#)]
142. Lindfors, T.; Ivaska, A. pH sensitivity of polyaniline and its substituted derivatives. *J. Electroanal. Chem.* **2002**, *531*, 43–52. [[CrossRef](#)]
143. Anothumakkool, B.; Soni, R.; Bhange, S.N.; Kurungot, S. Novel scalable synthesis of highly conducting and robust PEDOT paper for a high performance flexible solid supercapacitor. *Energy Environ. Sci.* **2015**, *8*, 1339–1347. [[CrossRef](#)]
144. Choi, H.; Ahn, K.-J.; Lee, Y.; Noh, S.; Yoon, H. Free-Standing, Multilayered Graphene/Polyaniline-Glue/Graphene Nanostructures for Flexible, Solid-State Electrochemical Capacitor Application. *Adv. Mater. Interfaces* **2015**, *2*, 1500117. [[CrossRef](#)]
145. Assresahegn, B.D.; Brousse, T.; Bélanger, D. Advances on the use of diazonium chemistry for functionalization of materials used in energy storage systems. *Carbon* **2015**, *92*, 362–381. [[CrossRef](#)]
146. Bensghaier, A.; Mousli, F.; Lamouri, A.; Postnikov, P.S.; Chehimi, M.M. The Molecular and Macromolecular Level of Carbon Nanotube Modification Via Diazonium Chemistry: Emphasis on the 2010s Years. *Chem. Afr.* **2020**, *3*, 535–569. [[CrossRef](#)]
147. Liu, X.; Shang, P.; Zhang, Y.; Wang, X.; Fan, Z.; Wang, B.; Zheng, Y. Three-dimensional and stable polyaniline-grafted graphene hybrid materials for supercapacitor electrodes. *J. Mater. Chem. A* **2014**, *2*, 15273–15278. [[CrossRef](#)]

148. Li, S.; Chen, Y.; He, X.; Mao, X.; Zhou, Y.; Xu, J.; Yang, Y. Modifying Reduced Graphene Oxide by Conducting Polymer Through a Hydrothermal Polymerization Method and its Application as Energy Storage Electrodes. *Nanoscale Res. Lett* **2019**, *14*, 226. [[CrossRef](#)] [[PubMed](#)]
149. Thomas, A.; Kuhn, P.; Weber, J.; Titirici, M.M.; Antonietti, M. Porous polymers: Enabling solutions for energy applications. *Macromol. Rapid Commun.* **2009**, *30*, 221–236. [[CrossRef](#)]
150. Zhou, C.; Gao, T.; Liu, Q.; Wang, Y.; Xiao, D. Preparation of quinone modified graphene-based fiber electrodes and its application in flexible asymmetrical supercapacitor. *Electrochim. Acta* **2020**, *336*, 135628. [[CrossRef](#)]
151. Lu, X.; Li, L.; Song, B.; Moon, K.-S.; Hu, N.; Liao, G.; Shi, T.; Wong, C. Mechanistic investigation of the graphene functionalization using p-phenylenediamine and its application for supercapacitors. *Nano Energy* **2015**, *17*, 160–170. [[CrossRef](#)]
152. Park, Y.T.; Grunlan, J.C. Carbon Nanotube-Based Multilayers. In *Multilayer Thin Films*; Wiley-VCH Verlag GmbH & Co. KGaA: Weinheim, Germany, 2012; pp. 595–612. [[CrossRef](#)]
153. Bhattacharyya, D.; Howden, R.M.; Borrelli, D.C.; Gleason, K.K. Vapor phase oxidative synthesis of conjugated polymers and applications. *J. Polym. Sci. Part B Polym. Phys.* **2012**, *50*, 1329–1351. [[CrossRef](#)]
154. Asatekin, A.; Barr, M.C.; Baxamusa, S.H.; Lau, K.K.S.; Tenhaeff, W.; Xu, J.; Gleason, K.K. Designing polymer surfaces via vapor deposition. *Mater. Today* **2010**, *13*, 26–33. [[CrossRef](#)]
155. Li, Q.; Horn, M.; Wang, Y.; MacLeod, J.; Motta, N.; Liu, J. A Review of Supercapacitors Based on Graphene and Redox-Active Organic Materials. *Materials* **2019**, *12*, 703. [[CrossRef](#)]
156. Gogotsi, Y.; Simon, P. True Performance Metrics in Electrochemical Energy Storage. *Science* **2011**, *334*, 917. [[CrossRef](#)]
157. Ramana, G.V.; Srikanth, V.V.S.S.; Padya, B.; Jain, P.K. Carbon nanotube–polyaniline nanotube core–shell structures for electrochemical applications. *Eur. Polym. J.* **2014**, *57*, 137–142. [[CrossRef](#)]
158. Wang, P.H.; Wang, T.L.; Lin, W.C.; Lin, H.Y.; Lee, M.H.; Yang, C.H. Enhanced Supercapacitor Performance Using Electropolymerization of Self-Doped Polyaniline on Carbon Film. *Nanomaterials* **2018**, *8*, 214. [[CrossRef](#)] [[PubMed](#)]
159. Gao, Z.; Wang, F.; Chang, J.; Wu, D.; Wang, X.; Wang, X.; Xu, F.; Gao, S.; Jiang, K. Chemically grafted graphene-polyaniline composite for application in supercapacitor. *Electrochim. Acta* **2014**, *133*, 325–334. [[CrossRef](#)]
160. Chang, H.-H.; Chang, C.-K.; Tsai, Y.-C.; Liao, C.-S. Electrochemically synthesized graphene/polypyrrole composites and their use in supercapacitor. *Carbon* **2012**, *50*, 2331–2336. [[CrossRef](#)]
161. Wei, H.; Wang, Y.; Guo, J.; Yan, X.; O'Connor, R.; Zhang, X.; Shen, N.Z.; Weeks, B.L.; Huang, X.; Wei, S.; et al. Electropolymerized Polypyrrole Nanocoatings on Carbon Paper for Electrochemical Energy Storage. *ChemElectroChem* **2015**, *2*, 119–126. [[CrossRef](#)]
162. Li, Y.; Zhou, M.; Wang, Y.; Pan, Q.; Gong, Q.; Xia, Z.; Li, Y. Remarkably enhanced performances of novel polythiophene-grafting-graphene oxide composite via long alkoxy linkage for supercapacitor application. *Carbon* **2019**, *147*, 519–531. [[CrossRef](#)]
163. Teng, H.; Song, J.; Xu, G.; Gao, F.; Luo, X. Nitrogen-doped graphene and conducting polymer PEDOT hybrids for flexible supercapacitor and electrochemical sensor. *Electrochim. Acta* **2020**, *355*, 136772. [[CrossRef](#)]
164. Liu, Z.; Zhou, H.; Huang, Z.; Wang, W.; Zeng, F.; Kuang, Y. Graphene covalently functionalized with poly(p-phenylenediamine) as high performance electrode material for supercapacitors. *J. Mater. Chem. A* **2013**, *1*, 3454–3462. [[CrossRef](#)]
165. Yang, W.; Zhou, H.; Huang, Z.; Li, H.; Fu, C.; Chen, L.; Li, M.; Liu, S.; Kuang, Y. In situ growth of single-stranded like poly(o-phenylenediamine) onto graphene for high performance supercapacitors. *Electrochim. Acta* **2017**, *245*, 41–50. [[CrossRef](#)]
166. N'Diaye, J.; Lian, K. Polymerized fuchsin and modified carbon nanotube electrodes for electrochemical capacitors. *Nano-Struct. Nano-Objects* **2018**, *15*, 173–179. [[CrossRef](#)]
167. Gholipour-Ranjbar, H.; Ganjali, M.R.; Norouzi, P.; Naderi, H.R. Electrochemical investigation of functionalized graphene aerogel with different amount of p-phenylenediamine as an advanced electrode material for supercapacitors. *Mater. Res. Express* **2016**, *3*, 075501. [[CrossRef](#)]
168. Bello, A.; Fabiane, M.; Momodu, D.Y.; Khamlich, S.; Dangbegnon, J.K.; Manyala, N. Functionalized graphene foam as electrode for improved electrochemical storage. *J. Solid State Electrochem.* **2014**, *18*, 2359–2365. [[CrossRef](#)]
169. Manjunatha, N.; Imadadulla, M.; Lokesh, K.S.; Venugopala Reddy, K.R. Synthesis and electropolymerization of tetra-[β -(2-benzimidazole)] and tetra-[β -(2-(1-(4-aminophenyl))benzimidazole)] embedded cobalt phthalocyanine and their supercapacitance behaviour. *Dyes Pigments* **2018**, *153*, 213–224. [[CrossRef](#)]
170. Sun, J.; Klechikov, A.; Moise, C.; Prodana, M.; Enachescu, M.; Talyzin, A.V. A Molecular Pillar Approach to Grow Vertical Covalent Organic Framework Nanosheets on Graphene: Hybrid Materials for Energy Storage. *Angew. Chem. Int. Ed.* **2018**, *57*, 1034–1038. [[CrossRef](#)] [[PubMed](#)]
171. Basnayaka, P.A.; Ram, M.K. A Review of Supercapacitor Energy Storage Using Nanohybrid Conducting Polymers and Carbon Electrode Materials. In *Conducting Polymer Hybrids*; Kumar, V., Kalia, S., Swart, H.C., Eds.; Springer International Publishing: Cham, Switzerland, 2017; pp. 165–192. [[CrossRef](#)]
172. Borenstein, A.; Hanna, O.; Attias, R.; Luski, S.; Brousse, T.; Aurbach, D. Carbon-based composite materials for supercapacitor electrodes: A review. *J. Mater. Chem. A* **2017**, *5*, 12653–12672. [[CrossRef](#)]
173. Poonam; Sharma, K.; Arora, A.; Tripathi, S.K. Review of supercapacitors: Materials and devices. *J. Energy Storage* **2019**, *21*, 801–825. [[CrossRef](#)]
174. Gul, H.; Shah, A.-u.-H.A.; Bilal, S. Fabrication of Eco-Friendly Solid-State Symmetric Ultracapacitor Device Based on Co-Doped PANI/GO Composite. *Polymers* **2019**, *11*, 1315. [[CrossRef](#)]

175. Gul, H.; Shah, A.-u.-H.A.; Krewer, U.; Bilal, S. Study on Direct Synthesis of Energy Efficient Multifunctional Polyaniline–Graphene Oxide Nanocomposite and Its Application in Aqueous Symmetric Supercapacitor Devices. *Nanomaterials* **2020**, *10*, 118. [[CrossRef](#)]
176. Zhu, J.; Xu, Y.; Wang, J.; Wang, J.; Bai, Y.; Du, X. Morphology controllable nano-sheet polypyrrole–graphene composites for high-rate supercapacitor. *Phys. Chem. Chem. Phys.* **2015**, *17*, 19885–19894. [[CrossRef](#)] [[PubMed](#)]
177. Wang, Z.; Zhu, M.; Pei, Z.; Xue, Q.; Li, H.; Huang, Y.; Zhi, C. Polymers for supercapacitors: Boosting the development of the flexible and wearable energy storage. *Mater. Sci. Eng. R Rep.* **2020**, *139*, 100520. [[CrossRef](#)]
178. Rogers, R.E.; Bardsley, T.L.; Weinstein, S.J.; Landi, B.J. Solution-phase adsorption of 1-pyrenebutyric acid using single-wall carbon nanotubes. *Chem. Eng. J.* **2011**, *173*, 486–493. [[CrossRef](#)]
179. Velasquez, J.D.; Tomczykowa, M.; Plonska-Brzezinska, M.E.; Chaur, M.N. Evaluation of the Covalent Functionalization of Carbon Nano-Onions with Pyrene Moieties for Supercapacitor Applications. *Materials* **2020**, *13*, 1141. [[CrossRef](#)]
180. Putri, A.D.; Chotimah, N.; Ujjain, S.K.; Wang, S.; Futamura, R.; Vallejos-Burgos, F.; Khoerunnisa, F.; Morimoto, M.; Wang, Z.; Hattori, Y.; et al. Charge-transfer mediated nanopore-controlled pyrene derivatives/graphene colloids. *Carbon* **2018**, *139*, 512–521. [[CrossRef](#)]
181. Wu, X.; Hong, J.J.; Shin, W.; Ma, L.; Liu, T.; Bi, X.; Yuan, Y.; Qi, Y.; Surta, T.W.; Huang, W.; et al. Diffusion-free Grotthuss topochemistry for high-rate and long-life proton batteries. *Nat. Energy* **2019**, *4*, 123–130. [[CrossRef](#)]
182. Miyake, T.; Rolandi, M. Grotthuss mechanisms: From proton transport in proton wires to bioprotonic devices. *J. Phys. Condens. Matter* **2015**, *28*, 023001. [[CrossRef](#)]
183. Mazari, S.A.; Ali, E.; Abro, R.; Khan, F.S.A.; Ahmed, I.; Ahmed, M.; Nizamuddin, S.; Siddiqui, T.H.; Hossain, N.; Mubarak, N.M.; et al. Nanomaterials: Applications, waste-handling, environmental toxicities, and future challenges—A review. *J. Environ. Chem. Eng.* **2021**, *9*, 105028. [[CrossRef](#)]
184. Doan, H.A.; Agarwal, G.; Qian, H.; Counihan, M.J.; Rodríguez-López, J.; Moore, J.S.; Assary, R.S. Quantum Chemistry-Informed Active Learning to Accelerate the Design and Discovery of Sustainable Energy Storage Materials. *Chem. Mater.* **2020**, *32*, 6338–6346. [[CrossRef](#)]
185. Schon, T.B.; McAllister, B.T.; Li, P.F.; Seferos, D.S. The rise of organic electrode materials for energy storage. *Chem. Soc. Rev.* **2016**, *45*, 6345–6404. [[CrossRef](#)] [[PubMed](#)]
186. Bo, Z.; Li, C.; Yang, H.; Ostrikov, K.; Yan, J.; Cen, K. Design of Supercapacitor Electrodes Using Molecular Dynamics Simulations. *Nano-Micro Lett.* **2018**, *10*, 1–23. [[CrossRef](#)] [[PubMed](#)]
187. N'Diaye, J.; Siddiqui, S.; Pak, K.L.; Lian, K. Layer-by-layer assembly of inorganic–organic molybdovanadogermanic (GeMoV)-polyluminal composite electrodes for capacitive charge storage. *J. Mater. Chem. A* **2020**, *8*, 23463–23472. [[CrossRef](#)]